View metadata, citation and similar papers at core.ac.uk

brought to you by CORE

provided by NASA Technical Reports Server

NATIONAL AERONAUTICS AND SPACE ADMINISTRATION

Technical Report No. 32-771

Electrostatic Charging and Discharging Models and Analysis for Ranger Spacecraft During Launch

George I. Cohn

N65-32869 (ACCESSION NUMBER)
40 (PAGES)
CR-64632 (NASA CR OR TMX OR AD NUMBER)
1 (THRU)
(CODE)
31 (CATEGORY)
FACILITY FORM 602

GPO PRICE $ _____

CSFTI PRICE(S) $ _____

Hard copy (HC) $2.00

Microfiche (MF) .50

ff 653 July 65

JET PROPULSION LABORATORY
CALIFORNIA INSTITUTE OF TECHNOLOGY
PASADENA, CALIFORNIA

August 1, 1965

NATIONAL AERONAUTICS AND SPACE ADMINISTRATION

Technical Report No. 32-771

Electrostatic Charging and Discharging Models and Analysis for Ranger Spacecraft During Launch

George I. Cohn

W. S. Shipley, Manager
Environmental Requirements Section

JET PROPULSION LABORATORY
CALIFORNIA INSTITUTE OF TECHNOLOGY
PASADENA, CALIFORNIA

August 1, 1965

[redacted]

Jet Propulsion Laboratory
California Institute of Technology

Prepared Under Contract No. NAS 7-100
National Aeronautics & Space Administration

CONTENTS

CONTENTS (Cont'd)

TABLES

FIGURES

FIGURES (Cont'd)

PREFACE

This Report was prepared for the Jet Propulsion Laboratory under Contract No. NAS 7-100, sponsored by the National Aeronautics and Space Administration, under the direction of A. J. Nalbandian. The author is employed at Quantum Engineering, Inc., Pasadena, California.

ABSTRACT

32869

Spacecraft can become charged by processes such as rocket motors exhausting electrically charged combustion products, triboelectrification, interception of drift currents, and photo and secondary emission. The charging is limited by various discharge mechanisms such as conduction via the ambient space charge, corona, and arcing. Discharges, and perhaps even charging, may be sufficiently rapid to induce pulses of significant size in various electrical circuits within the spacecraft despite substantial amounts of shielding. These pulses may actuate a device at an inappropriate time and may even result in its destruction. For example, actuation of a high-voltage power supply at an altitude for which the voltage breakdown strength of the air is near a minimum may allow arcing which can burn out the power supply. A preliminary investigation of this causal chain is pursued with the aid of circuit theory and field theory.

author

I. INTRODUCTION

Various electrification processes can cause large amounts of charge to appear on a spacecraft during launch. The charging process is limited by different types of electrical discharges. Strong electric and magnetic fields can be created by the charging and discharging processes. The metal shroud surrounding the *Ranger* forms a Faraday cage which shields the payload. However, this shielding is not perfect, and the resulting leakage couples electrical pulses into sensitive electronic devices and circuits in the payload.

The objective of the investigation reported here is to aid the assessment of whether or not the electrical pulses induced in the payload circuitry by charging or discharging processes are sufficiently large to (1) actuate any device when it should not be actuated or (2) cause any device not to be actuated when it should be. To support this objective, the charging and discharging phenomenologies are examined. This provides the basis for constructing approximate equivalent circuits, which are then analyzed. The pertinent properties of the induced electrical pulses are graphed against the circuit parameters, charging current, and breakdown voltage to facilitate extraction of numerical values. A preliminary analysis is also made of the charging current. However, considerable work remains to be done to determine the actual values of charging current, breakdown voltage, and circuit parameters.

II. CHARGING PHENOMENOLOGY

Spacecraft charging involves various combinations of two basic phenomena: (1) differential collection of one type of charge over the other and (2) flow phenomena to remove the noncollected charge to relatively large distances.

A. Basic Charge-Separation Mechanisms

In an ionized gas, or a solid conductor or semiconductor, two types of charges are present, and one type generally has greater mobility than the other. An object such as a conducting body, in contact with the plasma, can accumulate an excess of the more mobile charge. For the case of a conductor surrounded by an ionized gas, the electrons are more mobile than the positive ions, and hence, the conductor can accumulate an excess of electrons. The electric field created by the excess electrons on the object reduces the drift velocity of the electrons toward the object and increases the drift velocity of the positive ions. The accumulation of electrons continues until equilibrium is reached; i.e., equal amounts of positive and negative charge arrive at the object surface per unit time. Under these conditions, typical voltages to which the conductor may be charged may be anywhere from a fraction of a volt to a few volts. A similar phenomenon takes place when two solid objects touch one another. The differences in charge carrier mobilities can cause a net charge to be transferred from one object to the other, thereby creating the contact potential difference between the two objects.

B. Subsequent Charge-Separation Mechanisms

The above process is the basic step in electrostatic charging, but by itself it does not create large potential differences. To create large potential differences, a physical process is required to remove the uncollected charges mechanically to large distances from the object being charged. The agency which removes the uncollected charge performs mechanical work. This work is converted into electrostatic energy, which is stored in the electric field created by the separated charges. The greater the separation is made, the larger the potential difference becomes. Examples of agencies which remove the uncollected charge to large distances are the wind, in case of triboelectric charging of aircraft by ice crystals, and the moving belt in the case of a Van de Graaff generator. In the case of interest here, the rocket exhaust gases act as the Van de Graaff belt or, even more, like the wind.

C. Shielding

An additional factor that facilitates generation of large potential differences is a physical arrangement which substantially shields the small contact (or equivalent diffusion) potential difference so that they are not as readily cancelled out by the fields created by the separated charges. Faraday cages in the Van de Graaff generator provide such shielding. In the rocket motor, the combustion chamber and nozzle perform this function.

D. Electrostatic Potential Generated by Charging

Figure 1 depicts a spacecraft and rocket motor. The potential at some observation point (ρ_o, z_o) is

$$\xrightarrow{\text{linearity *}} \quad (1) \qquad V = V_E + V_S$$

where

$$\xrightarrow{\text{sym def}} \quad (2) \qquad V_E = \text{the potential created by the charge in rocket exhaust gases}$$

and

$$\xrightarrow{\text{sym def}} \quad (3) \qquad V_S = \text{the potential created by the charge on the spacecraft}$$

The potential created by the charge in the exhaust gas column is

$$\xrightarrow{\text{phys def}} \quad (4) \qquad V_E = \frac{1}{4\pi\epsilon}\iiint \frac{\rho_E}{r}\, d\Lambda$$

and the potential created by the charge on the surface of the spacecraft is

$$\xrightarrow{\text{phys def}} \quad (5) \qquad V_S = \frac{1}{4\pi\epsilon}\iint \frac{\rho_S}{r}\, dS$$

where

$$\xrightarrow{\text{sym def}} \quad (6) \qquad \rho_E = \text{the volume charge density in the exhaust gases}$$

and

$$\xrightarrow{\text{sym def}} \quad (7) \qquad \rho_S = \text{the surface charge density on the spacecraft}$$

*See Appendix A for an explanation of the arrow bookkeeping notation to the left of the equation numbers.

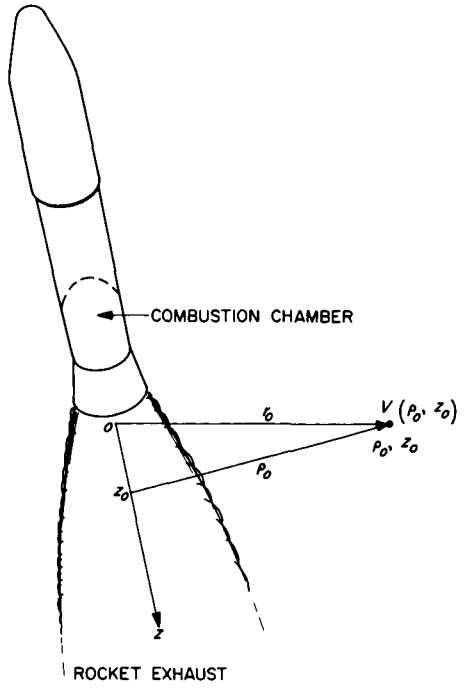

Fig. 1. Rocket-motor electrostatic generator

If the exhaust-gas column diameter is small compared to the distance of the observation point from the axis of symmetry, the volume integral can be approximated by a line integral

$$\xrightarrow{4} \quad (8) \qquad V_E = \frac{1}{4\pi\epsilon}\int_o^{z_{max}} \frac{Q_1(z)}{\sqrt{\rho_o^2 + (z - z_o)^2}}\, dz$$

If the spacecraft is sufficiently far away from other objects when the rocket motor is turned on and the time origin is taken at this instant, the end of the exhaust column is located at

$$\xrightarrow{\text{kinematics}} \quad (9) \qquad z_{max} = u_E t$$

where

$$\xrightarrow{\text{sym def}} \quad (10) \qquad u_E = \text{the exhaust-gas velocity with respect to the spacecraft}$$

The above formulation assumes that the exhaust-gas velocity is constant and that the spreading of and diffusion from the exhaust-gas column can be neglected. If the charge per unit length is also assumed to be

independent of position, it can be extracted from the integral, which then simplifies to

$$\xrightarrow[9,Q_1=\text{const}]{8} (11)$$

$$V_E = \frac{Q_1}{4\pi\epsilon} \ln \frac{\sqrt{(u_E t - z_o)^2 + \rho_o^2} + u_E t - z_o}{\sqrt{z_o^2 + \rho_o^2} - z_o}$$

The potential contributed by the surface charge on the spacecraft can be expressed by

$$\xrightarrow{5} (12) \qquad V_S = \frac{Q_s}{4\pi\epsilon r_o} F_S$$

where

$$\xrightarrow{\text{sym def}} (13) \qquad Q_S = \text{the total charge on the spacecraft}$$

and

$$\xrightarrow{\text{sym def}} (14) \qquad F_S = \text{a geometrical form factor which becomes unity for } r_o \text{ large compared to the spacecraft dimensions}$$

If the charge emission rate into the exhaust gases is a constant and charge neutralization is neglected, the total charge on the spacecraft can be expressed by

$$\xrightarrow{12} (15) \qquad Q_S = -Q_1 u_E t$$

The total potential can now be expressed by

$$\xrightarrow[11,\,12/15]{1} (16) \qquad V = -\frac{F_S Q_1 u_E}{4\pi\epsilon r_o} t + \frac{Q_1}{4\pi\epsilon} \ln \frac{\sqrt{(u_E t - z_o)^2 + \rho_o^2} + u_E t - z_o}{\sqrt{z_o^2 + \rho_o^2} - z_o}$$

For large values of time, the logarithm term can be neglected compared with the first term, which increases linearly with time. This equation shows that the potential (especially in the vicinity of the spacecraft) increases indefinitely with time and hence can build up to very large values. However, this linear increase with time cannot continue indefinitely.

E. Factors Limiting Potential Buildup

The assumptions employed in the derivation becomes increasingly inaccurate as time progresses. In particular, the charges diffuse out the gaseous exhaust column and are accelerated toward the spacecraft, thereby constituting a neutralizing current. In addition, the spacecraft may emit charge carriers which flow toward the exhaust-gas column, thus contributing to the neutralizing current. A third factor is that the unperturbed environment may be sufficiently conductive to support neutralizing currents. In several circumstances, such as staging and during launch, a significant part of the exhaust gases is deflected back to envelope the spacecraft. If the potential difference builds up sufficiently, electrical breakdown occurs. If neutralization did not take place, the electrostatic field would eventually build up until the leakage field into the basic charge-separation region becomes sufficient to cancel the charge-separating electromotance; then no further charge separation would occur. If the shielding about this region were sufficiently good, the electrostatic forces would eventually build up until the gas pressure forcing gas out of the rocket nozzle would be counterbalanced by the electrostatic attraction; then no further charged gas could be ejected. This would require unrealistically high insulation strength of the exhaust gas system and hence is not expected to occur.

The spacecraft charging current generated by the rocket motor

$$\xrightarrow{\text{B-4}} (17) \qquad I_g = Q_1 u_E$$

is derived in Appendix B. Currents of tens and even hundreds of milliamperes are possible on the basis of the model presented.

III. DISCHARGING PHENOMENOLOGY

The potential difference which can be obtained by the charging process described in Section II is limited by various types of discharging processes. These can be divided into three principal categories: (1) conduction (without the creation of new ions), (2) corona, and (3) arcing.

A. Spacecraft Ionized Gas Environment

The charge carriers contributing to the conduction processes originate from various sources. The original environment may contain electrons and ions which make the ambient media a conductor that can support current between the rocket exhaust column and the spacecraft. The electric fields generated by the separated charges cause the ions in the exhaust beam to be accelerated towards the spacecraft. These ions drag electrons along with them, which increases the conductivity of the intervening medium. There may be photoemission or high field intensity emission of electrons from sharp points or edges on the spacecraft, and these carriers contribute to the conductivity of the intervening medium. Gases, along with their constituent ions and electrons, also diffuse out of the rocket exhaust column. Part of this gas diffuses in the forward direction and even engulfs the spacecraft. While the fraction of the exhaust-gas mass that diffuses to and past the spacecraft may be a very small percentage of the total exhaust-gas mass, the effective contribution to the conductivity of the path between the exhaust column and the spacecraft may be significant. During staging, a much larger fraction of the exhaust-gas mass is deflected back towards the spacecraft. During takeoff, the ground deflects an even larger portion. Under these conditions, the rocket gases can provide the bulk of the immediate environment about the spacecraft.

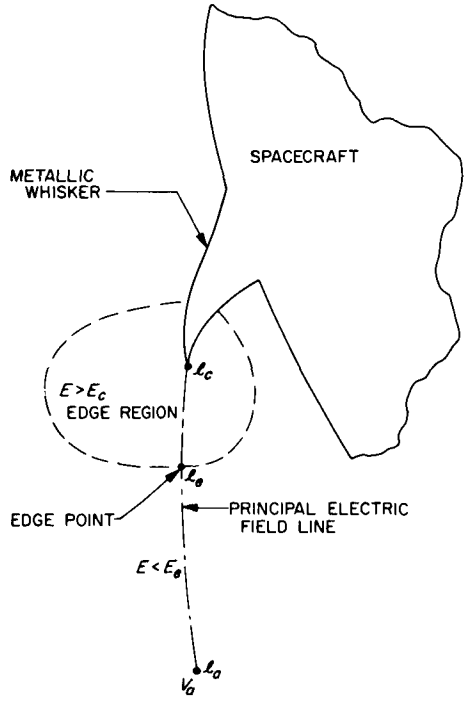

Fig. 2. Conditions defining electrical breakdown

B. Electrical Breakdown

If sufficient gas density exists in the spacecraft environment, electrical breakdown of this gas will result if the spacecraft potential exceeds a critical value. Breakdown can be initiated only in a region in which the electric field intensity is equal to or greater than a critical value E_c. The space in which the electric field intensity exceeds the critical value is called the edge region. An edge region is depicted in Fig. 2. The maximum potential difference across the edge region is called the edge voltage:

$$\xrightarrow{\text{phys def}} \quad (1) \qquad V_e = \left| \int_{l_c}^{l_e} \mathbf{E} \cdot d\mathbf{l} \right|$$

where the line integral is taken along the principal electric field line, i.e., the line along which the electric field intensity is a maximum with respect to any transverse direction. The point l_e divides the principal field line into two segments, such that $E > E_c$ over the segment within the edge region and $E < E_c$ over the segment outside the edge region. For convenience, the potential of the spacecraft is set equal to zero. The potential at any point within the region in which the exhaust beam is delivering space charge and to which a discharge may occur is designated by V_a. The edge point depends on the critical field, the charging current, and the geometry:

$$\xrightarrow{\text{causality}} \quad (2) \qquad l_e = l_e\,(E_c, I_g, \text{geometry})$$

Hence, the edge voltage also depends on these factors:

$$\xrightarrow[2]{1} \quad (3) \qquad V_e = V_e\,(E_c, I_g, \text{geometry})$$

When the edge voltage reaches some critical value V_{ec}, corona-type breakdown will occur. Solving for the critical generator current which will produce corona gives

$$\xrightarrow{3} \quad (4) \qquad I_{gc} = I_{gc}\,(E_c, V_{ec}, \text{geometry})$$

If the generator current is less than this critical value, equilibrium will be established and no breakdown will occur. In this type of equilibrium, the charging current I_g can be supported in the discharge path by charge carriers that move so slowly that relatively few new ion pairs are created. Corona breakdown occurs if the charging current exceeds this critical value but not the critical value at which an arc discharge occurs. This breakdown alters the edge region. In effect, it provides a conducting extension to the spacecraft edge which is not as sharp; hence, the new edge region about the initial phase of each coronal discharge is smaller than before. Each coronal discharge extends into its new edge region until the edge region vanishes, thereby halting the progress of the coronal discharge. The electrons generated in each coronal discharge are partly absorbed by molecules (particularly oxygen) to form negative ions with relatively low mobility and partly diffuse out into the ambient region. The positive ions in each coronal discharge are drawn toward the point from which the coronal discharge emanated. As the positive ions approach this point, the edge region becomes smaller and smaller until the particular coronal discharge is extinguished. The region just beyond the positive ions is occupied by the negative ions, which suppress the potential and keep a new coronal discharge from emanating from this point until the negative ions have sufficiently diffused or been swept away. At sea level, the individual coronal discharge pulses in air have an average duration of 0.2 μsec, with a rise time of 0.01 μsec.* The average discharge per pulse is approximately 10^{-9} coulombs. Corona discharge is comprised of a very large number of small pulses. These occur with sufficient frequency about the discharge region to give the appearance of a "corona."

Corona reduces the discharge path resistance by reducing the length of the high-resistance portion of the discharge path and by introducing more charge carriers into the path. The greater the amount by which the discharge current exceeds the critical value for initial corona formation, the larger the corona region. If the charging current exceeds the critical value by a sufficient amount for the corona region to extend into the heavily charged exhaust-gas region, flashover occurs and the spacecraft undergoes a sudden transient discharge.

*R. L. Tanner and J. E. Nanevicz, "An Analysis of Corona-Generated Interference in Aircraft," *Proceedings of the IEEE*, Vol. 52, No. 1, January 1964, pp. 44–52.

IV. EQUIVALENT CIRCUITS

A. Recurrent Networks for Representing Distributed Fields

An illustrative potential distribution and current flow distribution is depicted in Fig. 3 for a case in which the rocket exhaust flow is not disrupted and no breakdown discharge is present. Figure 4 illustrates a corresponding case, with corona discharge present. A recurrent equivalent circuit approximation can be obtained by subdividing the space into small subvolumes bounded by equipotential surfaces and current flow lines and representing each of these subvolumes by an elementary equivalent circuit. For the processes of interest here, it is adequate to represent each subvolume by a parallel combination of conductance and capacitance if the subvolume is passive, as depicted in Fig. 5. If the subvolume is active (i.e., contains a source of nonelectrical energy which can be converted to electrical energy, like the kinetic energy of the exhaust gases), an equivalent generator is required in the equivalent circuit, as shown in Fig. 5. The larger the

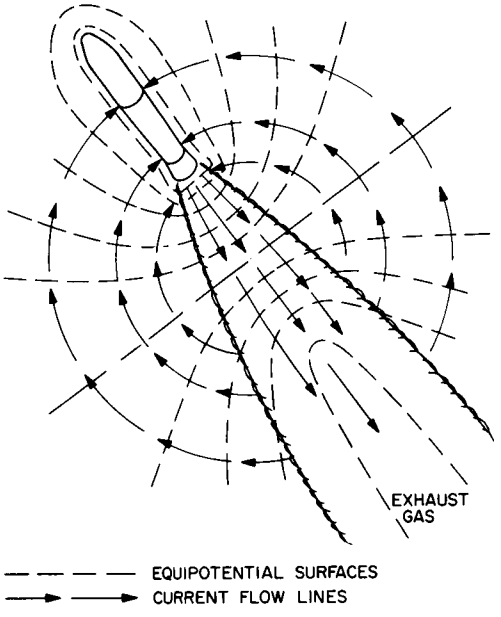

Fig. 3. Illustrative potential and current flow distribution

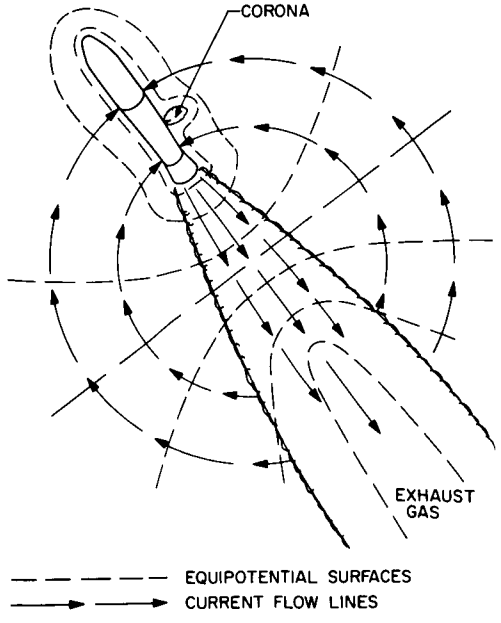

Fig. 4. Illustrative potential and current flow patterns with corona discharge

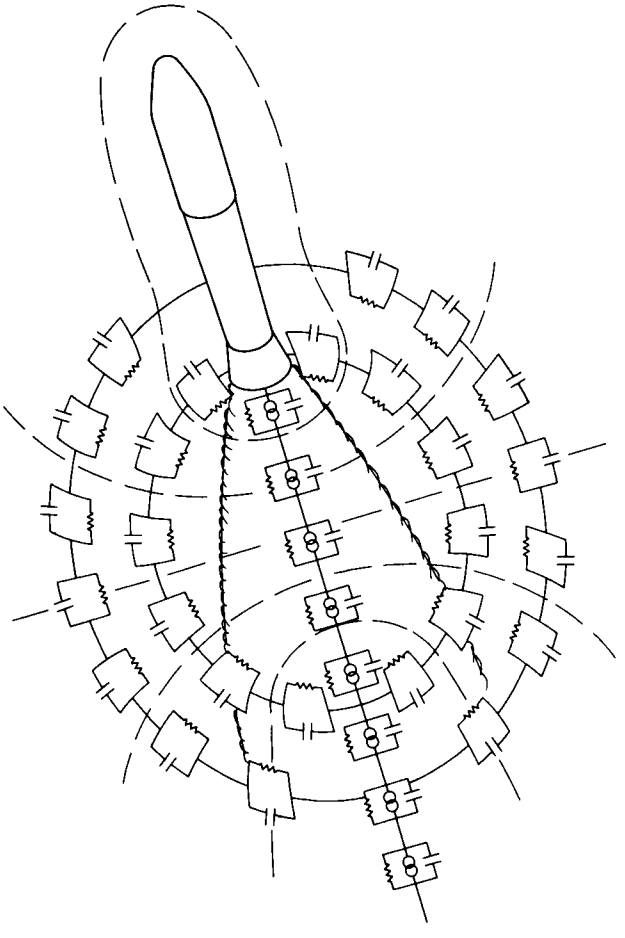

Fig. 5. An equivalent recurrent network for external charging and discharging

number of subvolumes used, the more accurate the representation, also the more laborious the analysis. It is desirable to use the simplest equivalent circuit which gives the required accuracy. The parameter values for the elements in each branch depend on the constituents in each subvolume being represented. The most appropriate division into subvolumes also depends on the overall distribution of charges. If the number of branches required in the equivalent circuit is excessive, it is more appropriate to analyze the problem with the original partial-differential field equations. Inductances are omitted from the equivalent circuit approximation used here. During the transient breakdown, inductive effects may be of importance. Inductive coupling is discussed in Section VIII.

B. Simplified Equivalent Circuits

A simplified equivalent circuit showing the entire passive portion reduced to a one-node-pair circuit and the entire active portion reduced to a one-node-pair circuit is depicted in Fig. 6. This circuit can be further reduced to that shown in Fig. 7.

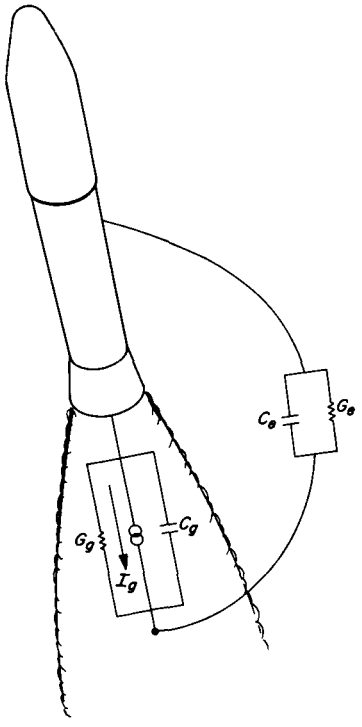

Fig. 6. Simplified equivalent circuit for spacecraft charging and discharging

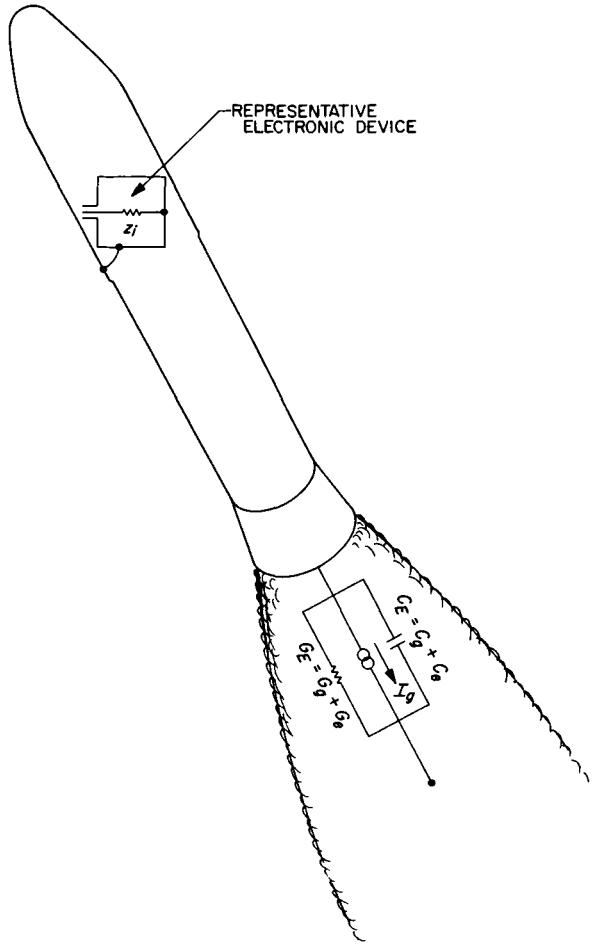

Fig. 7. Reduced equivalent circuit for external charging and discharging, with spacecraft payload isolated by shroud

The charging and discharging phenomena are of interest because of their effect on the internal electronic devices in the spacecraft. A representative electronic device is also shown in Fig. 7. The fields created by the charging and discharging processes can couple to the internal circuit via imperfections in the spacecraft shroud or hull, which thus does not act as a perfect Faraday cage. Figure 8 depicts an illustrative equipotential diagram, together with the leakage flux, for the case of an imperfection (large hole) in the shroud. An equivalent circuit, taking the capacitive and conductive coupling into account, is shown in Fig. 9. Inductive coupling and inductive effects are discussed later. This circuit is drawn in a more conventional form in Appendix D, where it is analyzed.

During a flashover discharge, the arc essentially short-circuits the external terminal pair, as shown in Fig. 9, by

closing the "equivalent switch" for flashover discharge. The resulting simplified circuit is redrawn in Appendix E, where it is analyzed.

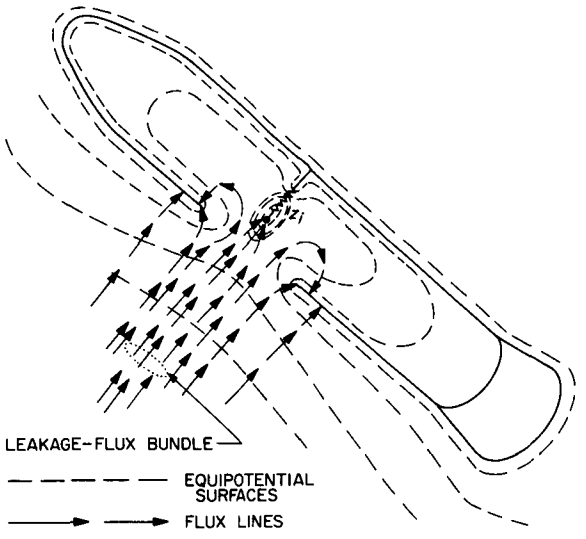

Fig. 8. Illustrative potential distribution and leakage-flux tube (hole-type imperfection in shroud grossly exaggerated for clarity)

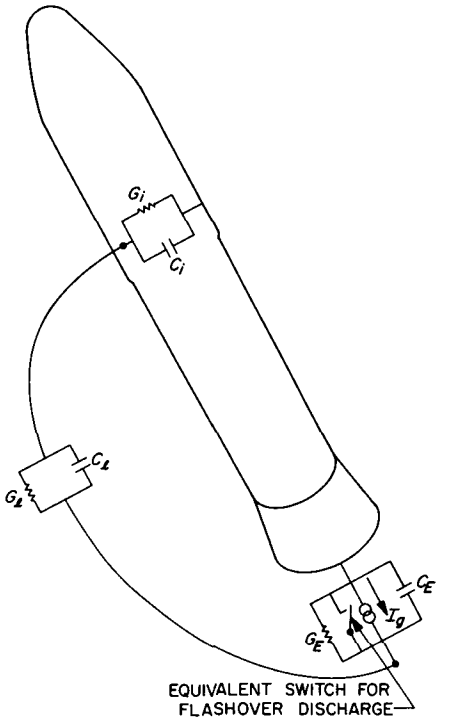

Fig. 9. Reduced equivalent circuit for charging and discharging, with coupling to an internal impedance

V. INDUCED VOLTAGE DURING THE CHARGING MODE

The simplified equivalent circuit for the charging mode is shown in Fig. 9 and, in a more conventional form, in Fig. D1 of Appendix D. Representing the external agency to (or from) which charge is transferred by a single-node-pair circuit may be a considerable oversimplification. Nevertheless, much information and insight can be provided by such a circuit. The analysis of this circuit is presented in Appendix D, together with the necessary universal curves, to facilitate extraction of numerical information once the system parameters are specified. Although not all system parameters under operating conditions are available, some measurements were made by W. R. Johnson and E. W. Beran of the Jet Propulsion Laboratory with an actual *Ranger* shroud in a modified setup without the rocket motors operating. The information obtained is reported in Interoffice Memo No. 3159-208 to W. S. Shipley, dated 29 June 1964. Data from Table I of this memo are reproduced here in Table 1. Table 1 also contains parameters computed from the data which are needed to utilize the results obtained in Appendix D. The ball-park estimates provided by Appendix C correspond reasonably well with the measured values of capacity.

In order to use Fig. D6 for estimating the peak voltage induced across the input terminals of an electronic device, it is necessary to determine $F(T_E)C_l/C_E$ to select the particular curve to be employed. The ratio C_l/C_E is also

Table 1. Equivalent circuit data

Umbilical pin	R_i, kΩ	C_i, μμf	C_l, μμf	C_i/C_E	C_l/C_E	τ_i μsec	C_l/C_i
3 t	3.0	2200	0.0314	9.17	1.31×10^{-4}	6.6	1.43×10^{-5}
3 m	2.0	2200	0.0314	9.17	1.31×10^{-4}	4.4	1.43×10^{-5}
4 W	3.3	1100	0.0157	4.58	0.654×10^{-4}	3.63	1.43×10^{-5}
3 n	500	1000	0.057	4.17	2.37×10^{-4}	500	5.7×10^{-5}
3 R	1000	800	0.0114	3.33	0.475×10^{-4}	800	1.43×10^{-5}
4 V	1000	500	0.036	2.08	1.50×10^{-4}	500	7.2×10^{-5}

$C_E = 240$ μμf for all umbilical pins.

given in Table 1 for the particular cases listed. The value of F can be obtained from Fig. D5 after T_E is determined from

$$\xrightarrow[\text{D-36}]{\text{D-47}} \quad (1) \qquad T_E = \frac{\tau_E}{\tau_i} = \frac{C_E G_i}{C_i G_E} = \frac{R_E C_E}{R_i C_i}$$

The values of C_i/C_E for the cases considered are also presented in Table 1.

The values of R_E were not determined but, under the experimental conditions, were extremely high. This would give

$$\xrightarrow{\text{experimental conditions}} \quad (2) \qquad \tau_E >> \tau_i$$

Consequently,

$$\xrightarrow{2} \quad (3) \qquad T_E >> 1$$

Hence, the value of F for these conditions, from Fig. D5, is essentially unity. The curves to be used in Fig. D6 for estimating the peak induced voltage are hence those having parameters in the range from about 0.4×10^{-4} to about 2.4×10^{-4}. Taking the $C_l\, C_E^{-1} = 10^{-4}$ curve as typical, the peak voltage is regraphed against input resistance for various values of charging current in Fig. 10. Thus, for a 1-meg input resistance, this means that the charging current must exceed 10 ma in order for the input peak voltage to exceed 1 v. For a 10kΩ input resistance, the charging current would have to exceed 1 amp in order to have the peak input voltage exceed 1 v.

The time it takes to reach the peak voltage is given by Fig. D3 or by

$$\xrightarrow{\text{D-53}} \quad (4) \qquad T_\wedge = \frac{1}{1 - T_E^{-1}} \ln \frac{T_l - 1}{T_l\, T_E^{-1} - 1}$$

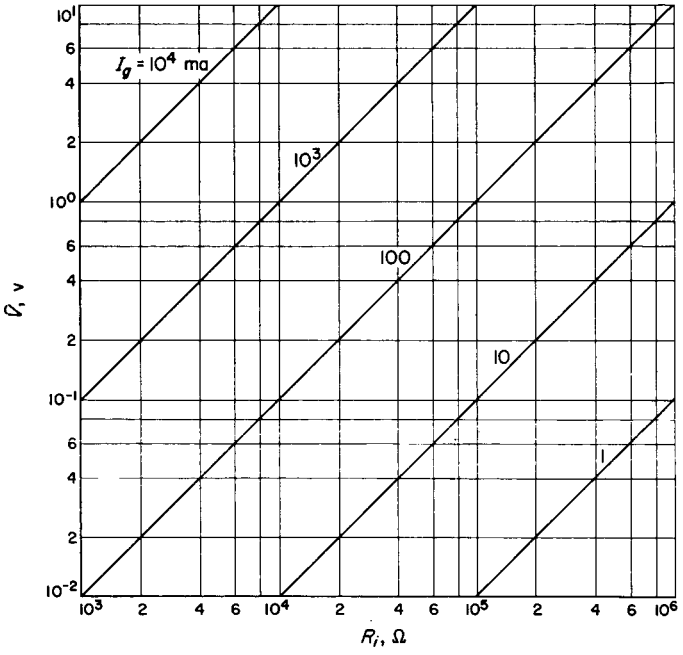

Fig. 10. Theoretical estimates for peak voltages developed across an input resistance for $C_E = 10^4\, C_l$

Under the conditions here

$$\xrightarrow[T_l > T_E >> 1]{4} \quad (5) \qquad T_\wedge = \ln T_E$$

Although T_E is unknown, even taking it as large as 10^6, only gives

$$\xrightarrow[T_E = 10^6]{5} \quad (6) \qquad T_\wedge = 13.8$$

Hence,

$$\xrightarrow{6,\ \text{D-47}} \quad (7) \qquad t_\wedge = 13.8\, \tau_i$$

Even for this extreme case, with the value of τ_i listed in Table 1, the maximum time to peak is only 11 msec. Thus, the peak voltage occurs right after the rocket motor is actuated and essentially before the rocket has lifted off the ground. Thus, if a breakdown or a false circuit actuation is going to occur *during charging*, it is most likely to be right at liftoff. Another factor which makes this likely is that the atmosphere is the densest at this point and hence has the greatest breakdown strength. If the maximum voltage to which the spacecraft could charge (in the absence of breakdown) exceeds the insulation breakdown strength of the external gases in the launch configuration, then the peak voltage which can be induced across the electronic circuit input terminals during the charging mode is correspondingly less. If the rocket were to fire after it has left the sensible atmosphere, then the breakdown strength would again be large. At some altitude in between, the breakdown strength is a minimum.

The peak voltage which may be induced during the discharge mode may be much greater than that induced during the charging mode because of the relative time constants in these two processes. The discharge mode is discussed in Section VI.

VI. DISCHARGING CIRCUIT ANALYSIS

The simplified equivalent circuit for the discharging mode is depicted in Fig. E1 of Appendix E. The analysis of this circuit is presented in Appendix E, together with the necessary universal curves to facilitate extraction of numerical information once the system parameters are specified. The C_l/C_i ratios for the cases considered in Section V are also listed in Table 1.

The principal part of the voltage generated on discharge is due to the charge stored in the leakage capacity during the charging mode being discharged through the input resistance in the discharge mode.

VII. FAILURE CRITERIA

Electrostatic charging or discharging of a spacecraft may conceivably produce malfunctions ranging from the physical destruction of a circuit to the actuation of a circuit at the wrong time. Conceivably, but less likely, the spurious signal generated by electrostatic charging or discharging may occur at such a time and be so poled as to prevent the proper signal from actuating the circuit. Spurious actuation is more likely to occur than direct circuit destruction, since far less energy is required. Actuation of a circuit at an inappropriate time may result in its destruction. For example, turning on a high-voltage power supply at an altitude at which the atmospheric pressure is too low (or not low enough) to provide adequate insulation may result in arcing and destruction of the power supply.

A. Failure-Criterion Pairs

For circuits whose untimely actuation constitutes a failure, the set of failure criteria is that which the spuriously generated signals must satisfy in order to actuate the circuit. Failure-criteria sets can be expressed in many forms. For example,

1. a. The input voltage must equal or exceed a critical value V_c AND

   b. it must do so for an interval of time equal to or greater than a critical time T_c in order to actuate the circuit.

If the voltage is below V_c, the circuit will not be actuated. If the voltage exceeds V_c but not for a sufficient time interval, the circuit will not be actuated.

An alternate pair of actuation (failure) criteria are the critical input current I_c and the critical time T_c. These criteria generally require further knowledge for reliable judgments to be obtained by their use. For example, if the input current or voltage is larger than the critical value, it is generally possible for the circuit to be actuated in a shorter time. The reduction in the critical actuation time is usually a function of the amount by which the input current or voltage exceeds the critical value. It is highly desirable to have failure criteria which are numerics rather than functions in order to simplify determination of failure danger domains.

A less variant set of failure criteria is provided by the critical voltage and the product of the critical voltage and the critical time (more generally, the time integral of the voltage over the critical time interval), or by the critical current and the product of the critical current and the critical time. The product of current and time is charge; hence, a more basic failure-criterion pair can be stated as follows:

2. a. The input current must equal or exceed the critical current I_c AND

   b. the input charge must equal or exceed the critical charge Q_c.

If the device actuation involves conversion of electrical to thermal energy or rectification, then a more appropriate pair of failure criteria may be:

3. a. The input power must equal or exceed the critical power P_c AND

   b. the input energy must equal or exceed the critical energy W_c.

B. Failure Domains

The ranges of circuit parameters and input conditions over which failure may occur can be obtained by examining the equation or the graphs of the electrical variables (voltage, current, charge) as a function of time. Because the number of parameters involved and the range of values over which these parameters should be considered are large, the amount of data to be handled by this approach may become excessive. The actual functions of time contain much more information than is required. A more compact representation of the required information can be provided by graphing only the peak values and/or the time durations over which the critical values are exceeded. The time it takes to reach a peak voltage can be used over certain parameter ranges as a rough estimate of the critical time. The range of conditions which may cause trouble can be mapped out on these graphs as domains. Since the peak voltage is maintained for zero time, the peak voltage must exceed the actuation voltage by a sufficient amount. Since the actuation time depends also on the amount by which the applied voltage exceeds the actuation voltage, it is difficult to utilize the time constant information properly. Consequently it is more convenient to utilize an integral of the current.

C. Charging Example

To illustrate the application of this type of failure criterion, consider the circuit for spacecraft charging an-

alyzed in Appendix D. The peak current which can flow through the input resistance is

$$\xrightarrow{\text{Ohm's Law}} \quad (1) \qquad \hat{I}_{R_i} = G_i \hat{V}_{Ii\infty}$$

For the case of negligible leakage conductance,

$$\xrightarrow[\text{D-63, D-64}]{1} \quad (2) \qquad \hat{I}_{R_i} = \frac{C_l}{C_i} F I_g$$

For this case, the maximum charge that can pass through R_i is just the charge which can accumulate on the leakage capacity when the full charging voltage is across it; thus,

$$\xrightarrow{\text{Fig D1}} \quad (3) \qquad \hat{Q}_{R_i} = C_l \hat{V}_E$$

The maximum voltage across the external part of the circuit occurs when all the generator current is flowing through the external conductance; hence,

$$\xrightarrow{\text{Fig D1}} \quad (4) \qquad \hat{V}_E = R_E I_g$$

The maximum charge through R_i can thus be expressed by

$$\xrightarrow[4]{3} \quad (5) \qquad \hat{Q}_{R_i} = C_l R_E I_g$$

The maximum current through R_i is therefore related to the maximum charge through R_i by

$$\xrightarrow[5]{2} \quad (6) \qquad \hat{I}_{R_i} = \frac{G_E}{C_i} F \hat{Q}_{R_i}$$

This is graphically represented in Fig. 11. As an example, consider a device which can be actuated by a current of 7 ma, provided that this current flows for at least 3 msec. Activation of this device requires a charge of at least 21 μcoulombs delivered at a minimum rate of 7 ma. Any combination of parameters which lie in the double cross-hatched area in Fig. 11 may actuate the device in the charging mode. For example, if $C_i R_E/F$ is 1 msec and $C_l R_E I_g$ exceed 21 μcoulombs, the device may be actuated. The actual failure region is smaller than the failure danger region because the peak current does not occur simultaneously with the peak charge. In fact, for the example considered, the current is zero when the charge is a maximum. If the current and charge were a simple exponential decay and buildup respectively, then the actual

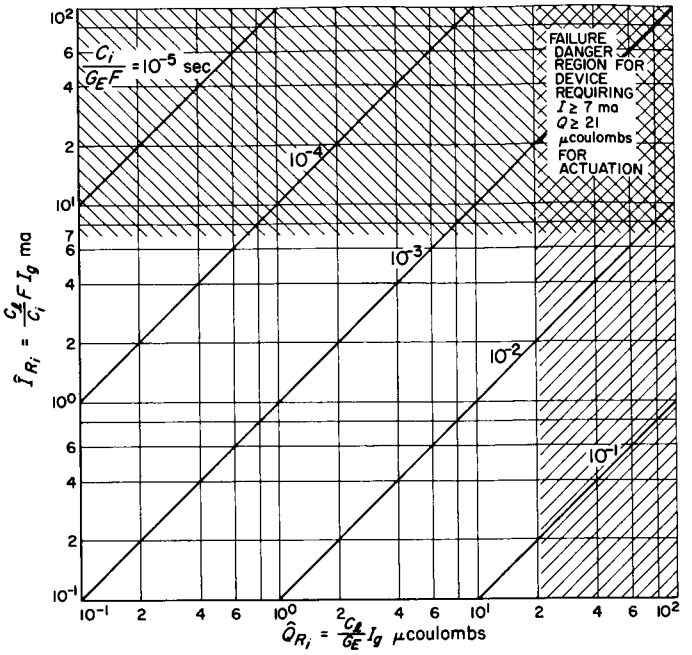

Fig. 11. Delineation of current-charge failure danger domain

failure region would have lower bounds (on the peak current and charge) of double the actual steady-state requirements for failure.

D. Discharging Example

Next consider the discharging mode. The peak voltage across R_i is the initial voltage, hence,

$$\xrightarrow{\text{E-16}} \quad (7) \qquad \hat{V}_{R_i} = \hat{V}_{io} = -\frac{C_l}{C_i} V_{EB-}$$

The peak charge is the asymptotic charge approached; hence,

$$\xrightarrow{\text{E-19}} \quad (8) \qquad \hat{Q}_{R_i} = \hat{Q}_{R_i\infty} = -C_l V_{EB-}$$

The peak voltage and charge are thus related by

$$\xrightarrow[7]{8} \quad (9) \qquad \hat{V}_{R_i} = \frac{1}{C_i} \hat{Q}_{R_i}$$

In order to compare different modes for failure likelihood, the same failure representations should be used for both. The peak current is related to the peak voltage by

$$\xrightarrow{\text{Ohm's Law}} \quad (10) \qquad \hat{I}_{R_i} = G_i \hat{V}_{R_i}$$

Consequently, the peak current is related to the peak charge by

$$\xrightarrow[9]{10} \quad (11) \qquad \hat{I}_{R_i} = \frac{G_i}{C_i} \hat{Q}_{R_i}$$

A set of characteristics can be graphed for this which are similar to those graphed for Eq. (6) in Fig. 11. The difference between these two sets is that in the characteristics for the discharge mode, G_i replaces $G_E F$ for the charging mode.

VIII. INDUCTIVE COUPLING FROM DISCHARGE CURRENTS

The large currents generated during a discharge build up in very short time intervals. The varying magnetic fields generated may penetrate the shroud and induce voltages in various circuits within the spacecraft. The objective of this Section is to provide an estimate on the upper bound of voltages which may be so induced. The voltage induced in a circuit is

$$\xrightarrow{\text{Faraday}} \quad (1) \qquad V = -\frac{d\Phi}{dt}$$

where

$$\xrightarrow{\text{sym def}} \quad (2) \quad \Phi = \text{the flux linking the circuit}$$

In terms of

$$\xrightarrow{\text{sym def}} \quad (3) \quad A = \text{the effective area of the circuit}$$

and

$$\xrightarrow{\text{sym def}} \quad (4) \quad \bar{B} = \text{the average flux density through the circuit}$$

the flux linking the circuit is

$$\xrightarrow{\text{phys def}} \quad (5) \qquad \Phi = A\bar{B}$$

Even though the geometry is complicated, an estimate for the flux density due to a concentrated discharge is provided by

$$\xrightarrow{\text{Ampere}} \quad (6) \qquad \bar{B} = \frac{\mu_v I}{4\pi r}$$

where

$$\xrightarrow{\text{sym def}} \quad (7) \quad r = \text{the effective distance of the circuit loop from the current } I$$

Since the circuit is shielded from the current source, it is necessary to use an isolation factor

$$\xrightarrow{\text{sym def}} \quad (8) \qquad K = e^{0.05\, db_{\text{isolation}}}$$

in (6), hence,

$$\xrightarrow[6,8]{} \quad (9) \qquad \bar{B} = \frac{\mu_v I}{2\pi r} K$$

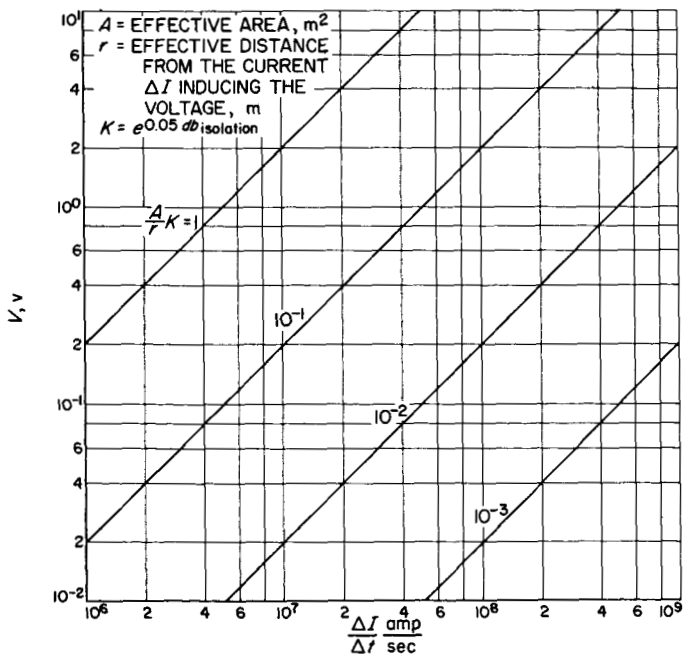

Fig. 12. Approximate inductively generated voltage in a circuit

The induced voltage is thus

$$\xrightarrow[5/9]{1} \quad (10) \qquad V = -\frac{\mu_v K A}{2\pi r}\frac{dI}{dt}$$

or

$$\xrightarrow[A\text{-}4]{10} \quad (11) \qquad V = -10^{-7}\frac{A}{r}K\frac{dI}{dt}$$

This is graphed in Fig. 12 against $\Delta I/\Delta t$ for various combinations of AK/r. For example, consider a circuit with an effective area of 100 cm^2 and a distance of 100 cm from a current discharge which increases to 600 amp in 2 μsec. The parameter value designating the particular characteristic to be used for this case is $AK/r = 10^{-2}$. Entering this curve at $\Delta I/\Delta t = 3 \times 10^8$ amp/sec gives an induced voltage of 0.6 v.

IX. CONCLUDING REMARKS

A. Summary

This Report

1. Examines the charging and discharging phenomenology
2. Develops equivalent circuits for analyzing the charging and discharging behavior of spacecraft and for determining the pulses induced at the input terminals of electronic circuits within the shroud
3. Develops an expression for the charging current
4. Analyzes the equivalent circuits to determine the induced voltages and currents at the input terminals of typical electronic circuits within the shroud
5. Partially formulates failure criteria

and, to a minor extent, discusses the inductive coupling and circuit parameters.

B. Numerical Information-Extraction Procedure for Particular Examples

The results obtained from analyzing the equivalent circuits and parameters are presented in graphical form to facilitate determination of numerical values for the induced voltages, currents, and charges.

1. Charging Behavior

The voltages for the charging model are given by Eq. (D28). If the charging cycle is assumed to start with quiescent initial conditions, the voltages reduce to Eq. (D-41). Of particular interest are

- $V_{Ii\infty}$ the asymptotic input voltage
- $t_\wedge$ the time it takes to reach the peak voltage
- $\hat{V}_{Ii}$ the peak value of the input voltage
- $\hat{V}^*_{Ii}$ the peak input voltage for the case in which the leakage conductance is negligible

These Quantities	*Can be obtained from Eq. or Fig.*		*Given the values of*
$V_{Ii\infty}$	(D-55)	D2	R_i, R_E, R_l, I_g
$T_\wedge$	(D-53)	D3	T_E, T_l
$\hat{V}_{Ii}/V_{Ii\infty}$	(D-57)	D4	T_E, T_l
$\hat{V}^*_{Ii}$	(D-63)	D6	$R_i, C_i, C_l, F, I_g, T_E$

The intermediate quantities in the righthand column are

F	given by Fig. D5 as a function of T_E	$\tau_E = R_E C_E$
$T_E = \tau_E/\tau_i$		$\tau_l = R_l C_l$
$T_l = \tau_l/\tau_i$		$\tau_i = R_i C_i$

Thus, R_i, R_E, R_l, C_i, C_E, C_l, and I_g comprise the basic set of quantities required to obtain numerical values for a particular charging case.

The charging current, based on a simplified model, is derived in Appendix B and is given by Eq. (B-21) and

Fig. B1. To obtain specific numerical values for a particular example from this equation or figure, it is necessary to know

- R the effective rocket-motor radius
- u_E the effective rocket-motor exhaust velocity
- T the effective electron temperature in the rocket motor
- n_e the effective electron density in the rocket motor

2. Discharging Behavior

The particular quantities of greatest interest in the discharge mode are

- $\hat{V}_{R_i}$ the peak value of the induced input voltage
- $\hat{Q}_{R_i}$ the peak value of the charge forced through R_i

These Quantities	*Can be obtained from Eq. or Fig.*	*Given the values of*
$\hat{V}_{io}$	(E-16) E2	C_i, C_l, V_{EB-}
$\hat{Q}_{R_i}$	(E-19) E3	C_l, V_{EB-}

Thus, C_i, C_l, and V_{EB-} comprise the basic set of quantities required to obtain numerical values for a particular discharging case.

The breakdown voltage phenomenology is presented in Section III. To obtain specific numerical values for a particular example, it is first necessary to analyze the proper model. Whatever the model, the following parameters will have to be substituted into the resulting equation:

- E_c the critical value of the electric field intensity which must be reached or exceeded before breakdown can occur
- V_{ec} the critical value of the edge voltage which must be reached or exceeded before breakdown can occur
- L_k the various geometrical dimensions of the model

C. Passive Ground Testing

The major inadequacy of passive ground testing is the absence of the hot ionized exhaust gases. This absence produces many simulation difficulties in both the charging mode and the discharging mode.

Expulsion of the exhaust gases is the prime cause of the charging current. To simulate this charging current, an external high-voltage generator is employed. This generator must simulate not only the ultimate charging voltage but also the charging current. The effects induced in the electronic circuits within the shroud are highly dependent on the charging current. Hence, using a generator whose charging current is an order of magnitude or more lower than the actual charging currents will produce test results which are also lower than the correct values by corresponding amounts. The external conductance during the charging cycle is strongly determined by the exhaust gases in actual operation. Consequently, it is difficult to determine the external conductance value to be employed in a static ground test. The leakage capacitance and external capacitance are not as severely affected by the exhaust gases, and hence their proper simulation is not as difficult.

The exhaust gases have the same importance in determining the external circuit parameters during discharging as during charging. Discharge conditions are even more difficult to simulate than charging conditions in passive ground tests. The principal difficulty lies in simulating the breakdown process. In actual operation, the most important discharge phenomenon appears to be the diffuse flashover observed in the exhaust gases. In the passive simulation, the corresponding discharge is a concentrated spark. Such concentrated sparks do not appear to have been observed in actual operation. The difference in the properties of these discharges reduces the validity of the results obtained by passive ground testing.

The magnitude of the effects induced in the circuits within the shroud as measured by passive ground testing is apt to be misleadingly small during the charging phase and misleadingly large during the discharging phase. During the charging phase, a major simulation inaccuracy results from the use of a generator with too small a current capability. In the discharge phase, the concentrated spark discharge is probably much faster than the actual diffuse flashover. In both phases, the external circuit values are apt to be in error.

D. Further Work Required

The results obtained by analyzing the equivalent circuits for charging and discharging are given in terms of the circuit parameters R_i, R_E, R_l, C_i, C_E, C_l, the charging current I_g, and the breakdown voltage V_{EB-}. These quantities must be numerically known for a specific example in order to determine the induced voltages, currents, and charges for the example. Quantities such as

1. R_i and C_i can be measured in a passive ground test and should be the same for active flight conditions
2. C_E and C_l have different values in a passive ground test than in active flight conditions, but the corresponding values should agree within a factor of the order of two

3. R_E, R_l, I_g, and V_{ER-} could have differences of many orders of magnitude between their active inflight and passive ground test conditions

The preliminary analysis for I_g given in this Report is based on what is expected to be the dominant mechanism for charging in a large number of cases. However, no confidence level can be assigned to this mechanism until the other mechanisms are analyzed and compared. The results obtained for the charging mechanism analyzed are in terms of other parameters such as exhaust velocity, electron temperature, and electron density, which still remain to be determined. The Report also discusses the voltage breakdown phenomena but does not provide analytical results to a depth corresponding to those for the charging current.

The most important specific items of work which should be pursued theoretically are the determination of

1. I_g, the charging current, specifically to include
   a. Determination of the charging current due to each of the six types of charging mechanisms listed in Appendix B and any other types of charging mechanisms which may occur. The total charging current is the sum of the individual charging currents. The relative importance of each charging mechanism depends on the fuel, rocket motor, and operating conditions.

      Investigation of some of the charging mechanisms may be dispensed with in the early stages of investigation based on certain basic criteria. Some cases may be adequately represented by a single charging mechanism. Confidence levels can be assigned to various charging mechanisms or groups of them once the overall analysis and comparison have been made.

   b. Determination of the effects on the charging currents of nonuniformity of temperature, density, and velocity in the rocket motor.

   c. Determination of the intermediate parameters such as temperature and density in terms of more normally specified characteristics of the rocket motor and fuel.

2. I_g, the charging current due to other causes specifically to include
   a. Determination of the charging current due to triboelectrification (similar to that encountered by aircraft) in passing through fields of particles. The voltages which can be built up by this cause are not expected to be as large as those caused by rocket motors.

   b. Determination of charging current due to the spacecraft passing through the ionosphere, the Van Allen belt, and through streams of particles in outer space. This charging takes place in the manner of a floating Langmuir probe and is expected to be relatively small.

3. V_{ER-}, the breakdown voltage, specifically to include
   a. Determination of the breakdown voltage for a simple geometrical model with a homogeneous medium in terms of the critical electric field strength and critical edge voltage.

   b. Determination of the critical electric field strength and critical edge voltage in terms of the exhaust-gas constituents.

   c. Determination of the deviations of the above due to nonuniformity for certain instructive cases.

4. G_E, the effective external conductance, specifically to include
   a. Determination of the external conductance for a simple model with a homogeneous medium.

   b. Determination of the external conductance for instructive nonhomogeneous cases of interest.

Additional items of importance are the determination of

1. G_l, the leakage conductance
2. C_l, the leakage capacitance
3. C_E, the external capacitance
4. The need for a more refined equivalent circuit for the various cases of interest.

APPENDIX A

Notation

I. DEVELOPMENT-TRACKING NOTATION

A special notation scheme is employed to increase the ease with which mathematical developments can be followed and, simultaneously, to simplify the process of committing them to written form with adequate detail. Arrows are placed to the left of each equation number to serve as a bookkeeping aid for the equation derivation. The information above each arrow designates the principal source or sources from which the equation originates. The information below the arrow refers to auxiliary sources of information or special conditions substituted into the primary sources in order to obtain the equation. Examples of the equation bookkeeping scheme, where the principal information source is one or more other equations, are given in Table A1.

Table A1. Bookkeeping scheme when principal sources for equations are in same Section

Example	Meaning
$\xrightarrow[10,\,11]{9}$ (12)	(12) is obtained by using (10) and (11) in (9)
$\xrightarrow{1+8}$ (9)	(9) is obtained by adding (1) and (8)
$\xrightarrow{17 \div 9}$ (31)	(31) is obtained by dividing (17) by (9)
$\xrightarrow[10/11]{9}$ (12)	(12) is obtained by substituting (11) into (10) and that result into (9)
$\xrightarrow[y \mp 3]{19}$ (41)	(41) is obtained by substituting $y = 3$ into (19)
$\xrightarrow[a << b]{8}$ (26)	(26) is obtained from (8) if $a << b$
$\xrightarrow[17;\,19]{12}$ (27)	Part one of (27) is obtained by substituting (17) into (12) and Part two of (27) is obtained by substituting (19) into (12)

Examples of the arrow bookkeeping scheme, where the principal source of information is not another equation, are given in Table A2.

Table A2. Bookkeeping scheme when sources are not equations

Example	Meaning
Fig 1 → (3)	(3) is obtained from the information in Fig. 1
Table 3 → (12)	(12) is obtained from the information in Table 3
causality → (2)	(2) is a basic cause-and-effect relationship
name → (5)	(5) is _____'s (name) law or equation
14 analog → (72)	(72) is obtained by a development analogous to the way in which (14) is obtained
sym def → (4)	(4) is a symbol definition
phys def → (6)	(6) is a physical definition
geom def → (8)	(8) is a geometrical definition
con def → (7)	(7) is a conceptual definition
identity → (9)	(9) is an identity
linearity → (13)	(13) is obtained by linear superposition of component parts

In each Section (or Appendix), the equations are independently numbered, starting from (1). Equations in the same Section (or Appendix) are referred to by number only, whereas the numbers of equations in a different Section (or Appendix) are preceded by the Section number (or Appendix letter). This is exemplified in Table A3.

Table A3. Bookkeeping scheme when source equations are in other Sections

Example	Meaning
9 → (12)	(12) is obtained from Eq. (9) in the same Section (or Appendix)
III-9 → (12)	(12) is obtained from Eq. (9) in Section III
F-9 → (12)	(12) is obtained from Eq. (9) in Appendix F

Material from other documents or papers are indicated as in Table A4.

Table A4. Bookkeeping scheme when sources are in other documents

Example	Meaning
Ref 3:132 → (12)	(12) is obtained from page 132 of Ref. 3
Ref 5(6–73) → (8)	(8) is obtained from Eq. (6–73) of Ref. 5

II. PHYSICAL CONSTANTS

		Quantity	*Name*
Ref 2:591 →	(1)	$c = 2.9978 \times 10^{8}$ m/sec	vacuum speed of light
Ref 2:591 →	(2)	$e = 1.6020 \times 10^{-19}$ coulombs $= 4.8028 \times 10^{-10}$ esu	electron charge
Ref 2:591 →	(3)	$\epsilon_v = 8.8552 \times 10^{-12}$ f/m $\cong \frac{1}{36\pi} \times 10^{-9}$ f/m	vacuum capacity
Ref 2:591 →	(4)	$\mu_v = 4\pi \times 10^{-7}$ h/m $\cong 1.2566 \times 10^{-6}$ h/m	vacuum inductivity
Ref 1:7-3 →	(5)	$m_e = 9.1085 \times 10^{-31}$ kg	electron mass
2, 5 →	(6)	$\frac{e}{m_e} = 1.7594 \times 10^{11}$ coulombs/kg	charge/mass ratio
Ref 1:7-3 →	(7)	$h = 6.6251 \times 10^{-34}$ j-sec $= 4.1355 \times 10^{-15}$ ev-sec $= 6.6251 \times 10^{-27}$ erg-sec	Planck's constant
Ref 1:7-3 →	(8)	$k = 1.3805 \times 10^{-23}$ joules/deg $= 8.6170 \times 10^{-5}$ ev/deg $= 1.3805 \times 10^{-16}$ erg/deg	Boltzmann's constant
Ref 1:7-3 →	(9)	$\sigma = 5.6697 \times 10^{-12}$ w-cm^{-2}-°K^{-4}	Stephan–Boltzmann constant

Ref 1:7-3 →	(10)	$N_A = 6.0248 \times 10^{23}$ molecules (g-mole)	Avogadro's number
Ref 1:7-3 →	(11)	$n_L = 2.6872 \times 10^{19}$ molecules/cc	Loschmidt's number
Ref 1:7-3 →	(12)	$M_1 = 1.6598 \times 10^{-27}$ kg	mass of particle with atomic weight one

III. SYMBOLS

A. Operator Symbols Placed on the Body-Symbol Level

Symbol	*Meaning*
d	differential
Δ	difference
$\lvert\ \rvert$	determinant
$\lvert\ \rvert$	absolute value
$\int$	integral

B. Symbols Placed Over the Body Symbol

Symbol	*Name*	*Meaning*
$\dot{}$	dot	derivative with respect to time
$\bar{}$	bar	Laplace transform, average
$\hat{}$	circumflex	maximum value
$\breve{}$	breve	minimum value

C. Symbols Placed Under the Body Symbol

Symbol	*Name*	*Meaning*
$\underline{\ }$	dash	matrix

D. Symbols in Superscript Position

Symbol	*Meaning*
$\downarrow$	functional or operator inverse

E. Symbols in Subscript Position

Symbol	*Meaning*
a	any arbitrary point
c	corner, critical
e	edge, electron, external
E	rocket exhaust
g	generator
i	input
l	leakage
o	observation point
s	plasma sheath
S	spacecraft
1	per unit length
$\hat{}$	argument value which maximizes function

F. Body Symbols

Symbol	*Meaning*
A	area
B	magnetic induction
C	capacitance
d	spacing, thickness or separation
E	electric field intensity

F	form factor	T	normalized time, temperature
G	conductance	u	velocity
I	current	V	voltage
K	isolation factor	z	axial rectalinear coordinate
l	length	ϵ	capacitivity
Q	charge	Λ	volume
r	radial distance from origin	μ	micro, permeability
R	resistance	π	circumference/diameter
s	time image parameter	ρ	charge density, radial distance from z-axis
S	surface area	τ	time constant
t	time	Φ	flux

APPENDIX B

Rocket-Motor Electrostatic Generator

I. INTRODUCTION

The objective of this Appendix is to provide ball-park estimates of

$\xrightarrow{\text{sym def}}$ (1) I_g = the charging current generated by the rocket motor

In terms of

$\xrightarrow{\text{sym def}}$ (2) u_E = the rocket-motor exhaust velocity

and

$\xrightarrow{\text{sym def}}$ (3) Q_1 = the charge per unit length of the rocket exhaust

the charging current is

$\xrightarrow{\text{phys def}}$ (4) $I_g = Q_1 u_E$

II. BASIC CHARGING MECHANISMS

There are many mechanisms by which the spacecraft can become charged via the agency of expelling exhaust gases from a rocket motor. For example:

1. The electrons can diffuse from the hot combustion products to the wall of the rocket motor. This process tends to make the spacecraft negative and the exhaust gases positive.
2. The positive ions can diffuse from the combustion products to the rocket-motor wall. This process tends to make the spacecraft positive and the exhaust gases negative. It is less dominant than process 1, above, unless almost all of the electrons are attached to form negative ions that are sufficiently heavier than the positive ions.
3. The rocket-motor wall may be sufficiently hot in spots to produce significant thermal electron emission. This process tends to make the spacecraft positive and the exhaust gases negative.
4. The rocket-motor wall may be sufficiently hot in spots so that significant contact ionization is produced. Some of the atoms and molecules which come into contact with the wall may deposit an electron and come away as positive ions. This process tends to make the spacecraft negative and the exhaust gases positive.
5. The combustion products may contain particles which come into contact with the rocket-motor wall and produce triboelectric charging. This charging may have either polarity, depending on the polarity of the contact potential between the rocket-motor wall and the particle.
6. The combustion gases may have a net charge because the fuel and oxidizer fed to the combustion chamber have a net charge. The net charge may be either positive or negative, depending on the contact potentials involved in the charging process.

In an actual case, the charging phenomena in all of these processes are expected to occur. Some of these charging phenomena may be negligible. The charging polarity will be determined primarily by the dominant process. The particular process which is dominant depends on the physical circumstances. Process 1 is the simplest and probably the most dominant process for a considerable variety of circumstances. This appendix analyzes the charging current due to process 1.

III. PLASMA-SHEATH CHARGING MODEL

The charge per unit length is the result of the electrons diffusing from the hot combustion products to the wall at a greater rate than the much heavier positive ions. This process creates a plasma sheath (adjacent to the rocket-motor wall) across which the electrostatic charging takes place. To simplify the analysis for the initial approximation, the rocket-motor combustion chamber and nozzle are approximated by a section of a uniform circular cylinder. In terms of

$\xrightarrow{\text{sym def}}$ (5) C_1 = the capacity of the plasma sheath per unit length of the cylinder

and

$\xrightarrow{\text{sym def}}$ (6) V_s = the potential difference developed across the plasma sheath by the electron temperature in the combustion products

the charge per unit length of the exhaust gas column is

$\xrightarrow{\text{con def of } C_1}$ (7) $$Q_1 = C_1 V_s$$

The charging current can now be expressed by

$$\xrightarrow[7]{4} \quad (8) \qquad I_g = C_1 V_s u_E$$

Since

$$\xrightarrow{\text{sym def}} \quad (9) \qquad d_s = \text{the plasma sheath thickness}$$

is very small compared to

$$\xrightarrow{\text{sym def}} \quad (10) \qquad R = \text{the rocket-motor radius}$$

the capacity across the plasma sheath can be computed as if it were a parallel-plate condenser. Consequently,

$$\xrightarrow{\text{C-8}} \quad (11) \qquad C_1 = \epsilon \frac{2\pi R}{d_s}$$

The voltage across the sheath is caused by the kinetic energy of the electrons obtained from their thermal motion. The electron gives up kinetic energy in crossing the potential difference across the sheath. The voltage which is developed by charge separation is that for which the potential energy gained by the electron in crossing the sheath is essentially equal to the average kinetic energy of the electrons; thus,

$$\xrightarrow{\text{energy conservation}} \quad (12) \qquad eV_s = kT$$

where

$$\xrightarrow{\text{sym def}} \quad (13) \qquad T = \text{the electron temperature}$$

Hence,

$$\xrightarrow{12} \quad (14) \qquad V_s = \frac{k}{e} T$$

The sheath thickness is approximately

$$\xrightarrow{\text{phys structure}} \quad (15) \qquad d_s = \text{the Debye radius}$$

which is given by

$$\xrightarrow{\text{Ref 3:97}} \quad (16) \qquad d_s = \sqrt{\frac{\epsilon kT}{n_e e^2}}$$

where

$$\xrightarrow{\text{sym def}} \quad (17) \qquad n_e = \text{number of electrons per cubic meter}$$

The capacity per unit length is consequently

$$\xrightarrow[16]{11} \quad (18) \qquad C_1 = 2\pi R e \sqrt{\frac{n_e \epsilon}{kT}}$$

hence, the charging current is

$$\xrightarrow[18,14]{8} \quad (19) \qquad I_g = 2\pi R \sqrt{n_e \epsilon k T}\, u_E$$

In this development, it is assumed that the rocket motor is sufficiently long for equilibrium to be established across the sheath during the exhaust-gas transit time through the rocket motor. Under these conditions, any additional length of rocket motor does not result in an increase in charging current. Hence, the length of the rocket motor does not appear in the above formula.

For the purpose of depicting this result graphically, it is convenient to consider the charging current generated per unit length of rocket-motor periphery:

$$\xrightarrow{19} \quad (20) \qquad \frac{I_g}{2\pi R} = \sqrt{\epsilon k T n_e}\, u_E$$

since this quantity is independent of the size of the rocket motor. Evaluating the numerical constants gives

$$\xrightarrow[\text{A-23, A-28}]{20} \quad (21) \qquad \frac{I_g}{2\pi R} = 1.1 \times 10^{-17} \sqrt{T n_e}\, u_E$$

This relationship is plotted in Fig. B1 against the exhaust-gas velocity for various combinations of the electron density and temperature.

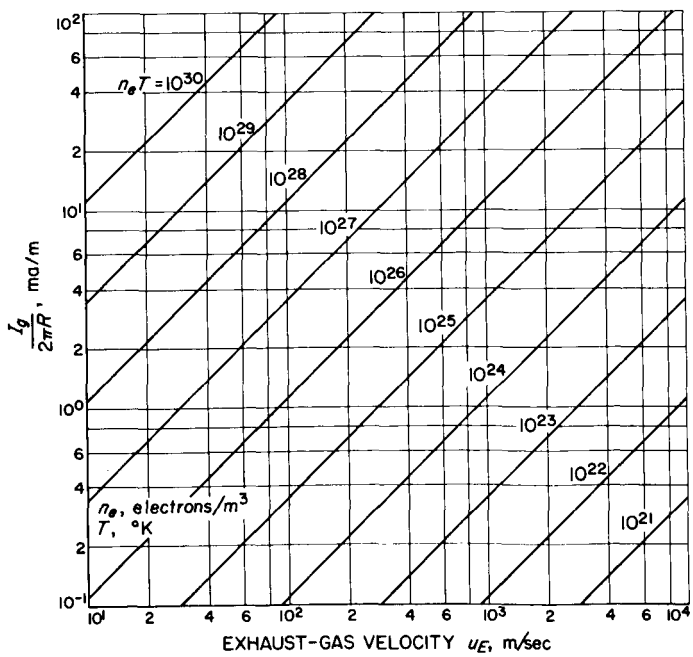

Fig. B1. Charging current per unit length of rocket-motor periphery vs exhaust-gas velocity for various temperature and electron density combinations

APPENDIX C

Capacitance Estimates

The complicated geometry makes the analytic determination of accurate capacitance values difficult. However, for the purposes of this investigation, objects with complicated shapes such as the spacecraft can be approximated by objects with simpler shapes without causing an order-of-magnitude error.

The capacitance of an isolated sphere is

$$\xrightarrow{\text{Ref 1:5-12}} \quad (1) \quad C_s = 4\pi\epsilon_v a = \frac{a}{9}\times 10^{-9}\ \text{f} = 111a\ \mu\mu\text{f}$$

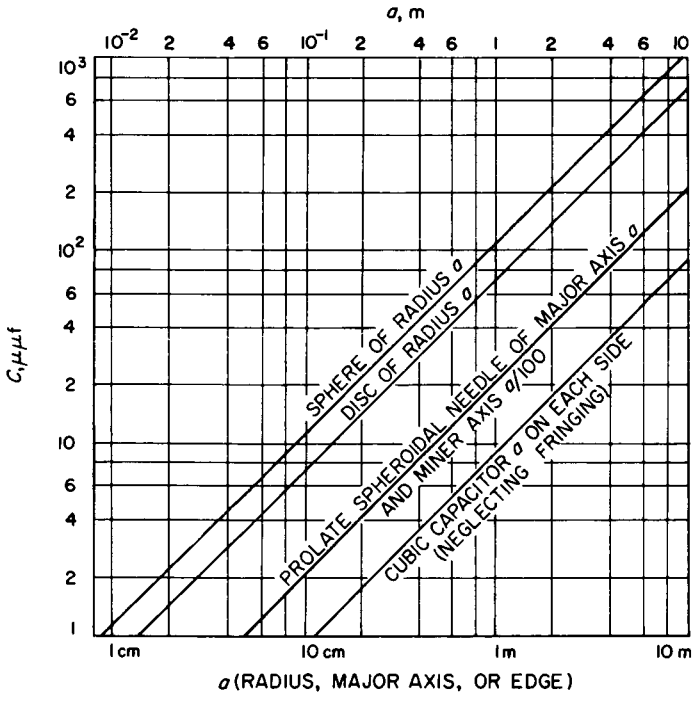

Fig. C1. Capacity of variously shaped objects

where a is the radius. This is graphed in Fig. C1. To provide an idea of how sensitive the capacity is to geometry, the capacities for oblate spheroids

$$\xrightarrow{\text{Ref 1:5-12}} \quad (2) \qquad C_{os} = \frac{4\pi\epsilon_v\sqrt{a^2 - b^2}}{\tan^{\downarrow}\sqrt{a^2 b^{-2} - 1}}$$

and prolate spheroids

$$\xrightarrow{\text{Ref 1:5-12}} \quad (3) \qquad C_{ps} = \frac{4\pi\epsilon_v\sqrt{b^2 - a^2}}{\tanh^{\downarrow}\sqrt{1 - a^2 b^{-2}}}$$

where b is the minor axis for the oblate spheroid and the major axis for the prolate spheroid, are also shown in Fig. C1. For the oblate spheroid,

$$\xrightarrow{1,2} \quad (4) \qquad \frac{C_{os}}{C_s} = \frac{\sqrt{1 - b^2 a^{-2}}}{\tan^{\downarrow}\sqrt{a^2 b^{-2} - 1}}$$

$$= \begin{cases} 0.828 & b = a/2 \\ 0.657 & b = a/10 \\ 0.635 & b = 0 \end{cases}$$

For the prolate spheroid,

$$\xrightarrow{1,3} \quad (5) \qquad \frac{C_{ps}}{C_s} = \frac{\sqrt{b^2 a^{-2} - 1}}{\tanh^{\downarrow}\sqrt{1 - a^2 b^{-2}}}$$

$$= \begin{cases} 1.315 & a = b/2 \\ 3.32 & a = b/10 \\ 18.9 & a = b/100 \end{cases}$$

Consequently,

$$\xrightarrow{4,1} \quad (6) \qquad C_{os} = \begin{cases} 92\,a\ \mu\mu\text{f} & b = a/2 \\ 73\,a\ \mu\mu\text{f} & b = a/10 \\ 70.5\,a\ \mu\mu\text{f} & b = 0 \end{cases}$$

and

$$\xrightarrow{5,1} \quad (7) \qquad C_{ps} = \begin{cases} 73\,b\ \mu\mu\text{f} & a = b/2 \\ 36.9\,b\ \mu\mu\text{f} & a = b/10 \\ 21\,b\ \mu\mu\text{f} & a = b/100 \end{cases}$$

Some of these capacities are plotted in Fig. C1 for comparison. The capacitance of a parallel-plate capacitor of area A and separation a, neglecting fringing, is

$$\xrightarrow{\text{Ref 2:29}} \quad (8) \quad C_{\shortparallel} = \epsilon_v\frac{A}{a} = \frac{10^{-9}}{36\pi}\frac{A}{a}\ \text{f} = 8.83\frac{A}{a}\ \mu\mu\text{f}$$

The capacitance of a cubic condenser, a on each side, neglecting fringing, is thus

$$\xrightarrow[A = a^2]{8} \quad (9) \qquad C = 8.83a\ \mu\mu\text{f}$$

as shown graphically in Fig. C1.

APPENDIX D

Analysis of Two-Node Pair RC Equivalent Charging Circuit

I. CIRCUIT EQUATIONS

The objective of this Appendix is to assess the voltage induced across the input terminals of typical electronic devices during charging conditions by using the two-node-pair RC equivalent circuit to approximate the system. This equivalent circuit is depicted in Fig. D1. Kirchoff's node equations are

Fig D1 node E →

$$(1)\quad I_g = G_E V_E + C_E \dot{V}_E + G_l (V_E - V_i) + C_l (\dot{V}_E - \dot{V}_i)$$

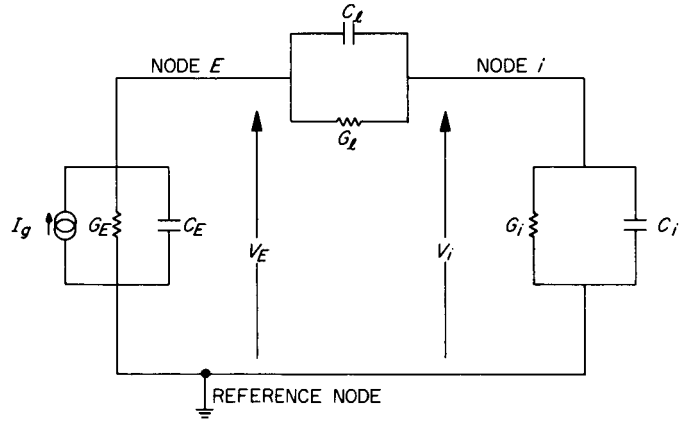

Fig. D1. Equivalent circuit for analysis of voltage induced across an input circuit during charging mode

and

Fig D1 node i →

$$(2)\quad 0 = G_i V_i + C_i \dot{V}_i + G_l (V_i - V_E) + C_l (\dot{V}_i - \dot{V}_E)$$

In time intervals comparable to the circuit time constants, the variation of equivalent circuit parameters with time is assumed to be small. The circuit can be analyzed as a fixed-parameter circuit without inducing significant errors when this assumption is valid. The approximation is probably valid over the intervals between electrical breakdowns but not during the breakdowns.

The circuit equations can be expressed in the more compact matrix form

1, 2 →

$$(3)\quad \begin{vmatrix} G_{ii} + C_{ii}\frac{d}{dt} & -G_l - C_l\frac{d}{dt} \\ -G_l - C_l\frac{d}{dt} & G_{EE} + C_{EE}\frac{d}{dt} \end{vmatrix} \begin{vmatrix} V_i \\ V_E \end{vmatrix} = \begin{vmatrix} 0 \\ I_g \end{vmatrix}$$

where

sym def →

$$(4)\quad \begin{vmatrix} G_{ii} & C_{ii} \\ G_{EE} & C_{EE} \end{vmatrix} = \begin{vmatrix} G_i + G_l & C_i + C_l \\ G_E + G_l & C_E + C_l \end{vmatrix}$$

II. SOLUTION BY LAPLACE TRANSFORMS

Taking the Laplace transform of the circuit equations gives

$$\xrightarrow{4,\ \text{Tab D1}} \quad (5) \quad \begin{vmatrix} a_{ii} & a_{iE} \\ a_{Ei} & a_{EE} \end{vmatrix} \begin{vmatrix} \bar{V}_i \\ \bar{V}_E \end{vmatrix} = \begin{vmatrix} Q_{ii} \\ Q_{EE} + \frac{1}{s} I_g \end{vmatrix}$$

Table D1. Laplace transform pairs

No.	Original function	Transform function
1	$f(t)$	$\bar{f}(s) = \int_0^\infty e^{-st} f(t)\,dt$
2	K	$\frac{K}{s}$
3	$f'(t)$	$s\bar{f}(s) - f(0)$
4	e^{at}	$\frac{1}{s-a}$

where

$$\xrightarrow{\text{sym def}} \quad (6) \quad \begin{vmatrix} a_{ii} & a_{iE} \\ a_{Ei} & a_{EE} \end{vmatrix} = \begin{vmatrix} G_{ii} + C_{ii}s & -G_l - C_l s \\ -G_l - C_l s & G_{EE} + C_{EE}s \end{vmatrix}$$

and where the Q's represent the initial charge conditions given by

$$\xrightarrow{\text{sym def}} \quad (7) \quad \begin{vmatrix} Q_{ii} \\ Q_{EE} \end{vmatrix} = \begin{vmatrix} -C_{ii} V_i(0) + C_l V_E(0) \\ C_l V_i(0) - C_{EE} V_E(0) \end{vmatrix}$$

Solving for the voltage transforms gives

$$\xrightarrow{5} \quad (8) \quad \begin{vmatrix} \bar{V}_1 \\ \bar{V}_2 \end{vmatrix} = \begin{vmatrix} a_{ii} & a_{iE} \\ a_{Ei} & a_{EE} \end{vmatrix}^{-1} \begin{vmatrix} Q_{ii} \\ Q_{EE} + \frac{1}{s} I_g \end{vmatrix}$$

Taking the matrix inverse yields

$$\xrightarrow{\text{sym def}} \quad (9) \quad \begin{vmatrix} \bar{V}_1 \\ \bar{V}_2 \end{vmatrix} = \frac{1}{|\underline{a}|} \begin{vmatrix} a_{EE} & -a_{iE} \\ -a_{Ei} & a_{ii} \end{vmatrix} \begin{vmatrix} Q_{ii} \\ Q_{EE} + \frac{1}{s} I_g \end{vmatrix}$$

where the determinant of the coefficients is

$$\xrightarrow{\text{sym def}} \quad (10) \qquad |\underline{a}| = a_{ii}a_{EE} - a_{iE}a_{Ei}$$

To obtain the inverse transforms, the explicit functional dependence on the image parameter is required:

$$\xrightarrow[6]{9} \quad (11) \quad \begin{vmatrix} \bar{V}_1 \\ \bar{V}_2 \end{vmatrix} = \frac{1}{|\underline{a}|} \begin{vmatrix} G_{EE} + C_{EE}s & G_l + C_l s \\ G_l + C_l s & G_{ii} + C_{ii}s \end{vmatrix} \begin{vmatrix} Q_{ii} \\ Q_{EE} + \frac{1}{s} I_g \end{vmatrix}$$

Expressing the determinant explicitly gives

$$\xrightarrow[6]{10} \quad (12) \qquad |\underline{a}| = (G_{ii} + C_{ii}s)(G_{EE} + C_{EE}s) - (G_l + C_l s)^2$$

Using

$$\xrightarrow{\text{sym def}} \quad (13) \qquad K = C_{ii}C_{EE} - C_l^2$$

and

$$\xrightarrow{\text{sym def}} \quad (14) \quad \begin{vmatrix} -2b \\ C \end{vmatrix} = \frac{1}{K} \begin{vmatrix} C_{ii}G_{EE} + C_{EE}G_{ii} - 2C_l G_l \\ G_{ii}G_{EE} - G_l^2 \end{vmatrix}$$

yields

$$\xrightarrow[13,14]{12} \quad (15) \qquad |\underline{a}| = K[s^2 - 2bs + C]$$

Factoring gives

$$\xrightarrow{15} \quad (16) \qquad |\underline{a}| = K(s - s_1)(s - s_2)$$

where

$$\xrightarrow{\text{sym def}} \quad (17) \qquad s_{1,2} = b \pm \sqrt{b^2 - C}$$

Expressing the various parameters more explicitly in terms of the circuit parameters gives

$$\xrightarrow[4]{13} (18) \qquad K = C_iC_E + C_iC_l + C_EC_l$$

and

$$\xrightarrow[4]{14} (19) \qquad \begin{vmatrix} -2b \\ C \end{vmatrix} = \frac{1}{K} \begin{vmatrix} C_EG_i + C_EG_l + C_lG_i + C_iG_E + C_lG_E + C_iG_l \\ G_iG_E + G_iG_l + G_EG_l \end{vmatrix}$$

Separating the voltage transforms into the various functions of the image parameter and carrying out the inversion is facilitated by using the more compact matrix expressions

$$\xrightarrow{\text{sym def}} (20) \qquad \underline{\bar{V}} = \begin{vmatrix} \bar{V}_1 \\ \bar{V}_2 \end{vmatrix}$$

$$\xrightarrow{\text{sym def}} (21) \qquad \underline{Q} = \begin{vmatrix} Q_{ii} \\ Q_{EE} \end{vmatrix}$$

$$\xrightarrow{\text{sym def}} (22) \qquad \underline{I} = \begin{vmatrix} 0 \\ I_g \end{vmatrix}$$

$$\xrightarrow{\text{sym def}} (23) \qquad \underline{G} = \begin{vmatrix} G_{EE} & G_l \\ G_l & G_{ii} \end{vmatrix}$$

and

$$\xrightarrow{\text{sym def}} (24) \qquad \underline{C} = \begin{vmatrix} C_{EE} & C_l \\ C_l & C_{ii} \end{vmatrix}$$

In terms of these, the circuit transform matrix equation is

$$\xrightarrow[20,\ 21,\ 22,\ 23,\ 24]{11} (25) \qquad \underline{\bar{V}} = \frac{1}{|\underline{a}|}[\underline{G} + \underline{C}s]\left[\underline{Q} + \underline{I}\frac{1}{s}\right]$$

Separating this into component functions of the image parameter gives

$$\xrightarrow{25} (26) \qquad \underline{\bar{V}} = \frac{1}{s|\underline{a}|}\underline{GI} + \frac{1}{|\underline{a}|}[\underline{GQ} + \underline{CI}] + \frac{s}{|\underline{a}|}\underline{CQ}$$

Table D2. Partial fraction expansions

No.	Fraction	Expansion
1	$\frac{1}{(s-s_1)(s-s_2)}$	$\frac{1}{s_1-s_2}\left[\frac{1}{s-s_1} - \frac{1}{s-s_2}\right]$
2	$\frac{s}{(s-s_1)(s-s_2)}$	$\frac{1}{s_1-s_2}\left[\frac{s_1}{s-s_1} - \frac{s_2}{s-s_2}\right]$
3	$\frac{1}{s(s-s_1)(s-s_2)}$	$\frac{1}{s_1s_2s} + \frac{1}{s_1-s_2}\left[\frac{s_1^{-1}}{s-s_1} - \frac{s_2^{-1}}{s-s_2}\right]$

Expanding in partial fractions,

$$\xrightarrow[16,\ \text{Tab D2}]{26} (27) \quad \underline{\bar{V}} = \frac{1}{Ks_1s_2s}\underline{GI} + \frac{1}{K(s_1-s_2)(s-s_1)}\left[\frac{1}{s_1}\underline{GI} + \underline{GQ} + \underline{CI} + s_1\underline{CQ}\right] + \frac{1}{K(s_1-s_2)(s-s_2)}\left[-\frac{1}{s_2}\underline{GI} - \underline{GQ} - \underline{CI} - s_2\underline{CQ}\right]$$

Taking the inverse transform gives

$$\xrightarrow[\text{Tab D1}]{27} (28) \quad \underline{V(t)} = \frac{1}{Ks_1s_2}\underline{GI} + \frac{1}{K(s_1-s_2)}\left[\frac{1}{s_1}\underline{GI} + \underline{GQ} + \underline{CI} + s_1\underline{CQ}\right]e^{s_1t} - \frac{1}{K(s_1-s_2)}\left[\frac{1}{s_2}\underline{GI} + \underline{GQ} + \underline{CI} + s_2\underline{CQ}\right]e^{s_2t}$$

It is convenient to consider separately the part due to the initial conditions

$$\xrightarrow{28,\ \text{def}} (29) \qquad \underline{V_Q(t)} = \frac{1}{K(s_1-s_2)}\{(\underline{G} + s_1\underline{C})e^{s_1t} - (\underline{G} + s_2\underline{C})e^{s_2t}\}\underline{Q}$$

and the part due to the driving current

$$\xrightarrow{28,\ \text{def}} (30) \quad \underline{V_I(t)} = \frac{1}{K}\left\{\frac{1}{s_1s_2}\underline{G} + \frac{1}{s_1-s_2}\left[\left(\frac{1}{s_1}\underline{G} + \underline{C}\right)e^{s_1t} - \left(\frac{1}{s_2}\underline{G} + \underline{C}\right)e^{s_2t}\right]\right\}\underline{I}$$

The total solution is

$$\xrightarrow[29,\ 30]{28} (31) \qquad \underline{V(t)} = \underline{V_I(t)} + \underline{V_Q(t)}$$

III. PRACTICAL SIMPLIFYING APPROXIMATIONS

For the practical cases of interest here,

$$\xrightarrow[\text{leakage}]{\text{small}} (32) \qquad C_E >> C_l << C_i$$

and

$$\xrightarrow[\text{leakage}]{\text{small}} (33) \qquad G_E >> G_l << G_i$$

Hence, for small leakage,

$$\xrightarrow[32]{18} (34) \qquad K = C_i C_E$$

and

$$\xrightarrow[32,33,34]{19} (35) \qquad \begin{vmatrix} -2b \\ C \end{vmatrix} = \frac{1}{C_i C_E} \begin{vmatrix} C_E G_i + C_i G_E \\ G_i G_E \end{vmatrix}$$

Small leakage means small coupling, which, in turn, means that the internal and external circuits behave essentially as if uncoupled in responding to initial condition. Hence, each circuit responds essentially with its own time constant. As a consequence, it is convenient to use the time constants

$$\xrightarrow{\text{sym def}} (36) \qquad \begin{vmatrix} \tau_i \\ \tau_E \end{vmatrix} = \begin{vmatrix} C_i/G_i \\ C_E/G_E \end{vmatrix}$$

Expressing the parameters in terms of these time constants gives

$$\xrightarrow[36]{35} (37) \qquad \begin{vmatrix} -2b \\ C \end{vmatrix} = \begin{vmatrix} \tau_i^{-1} + \tau_E^{-1} \\ \tau_i^{-1}\,\tau_E^{-1} \end{vmatrix}$$

The roots of the determinant are, consequently,

$$\xrightarrow[37]{17} (38) \qquad s_{1,2} = -\frac{\tau_i^{-1} + \tau_E^{-1}}{2} \pm \sqrt{\left(\frac{\tau_i^{-1} + \tau_E^{-1}}{2}\right)^2 - \tau_i^{-1}\,\tau_E^{-1}}$$

Hence,

$$\xrightarrow{38} (39) \qquad \begin{vmatrix} s_1 \\ s_2 \end{vmatrix} = -\begin{vmatrix} \tau_i^{-1} \\ \tau_E^{-1} \end{vmatrix}$$

The driven behavior is of prime importance during the charging mode. Considerations here are restricted to the case for which the leakage is small. For this case,

$$\xrightarrow[39]{30} (40) \qquad \underline{V_l(t)} = \frac{\tau_i\,\tau_E}{K}\left\{\underline{G} + \frac{1}{\tau_i - \tau_E}\left[(-\tau_i\,\underline{G} + \underline{C})e^{-t/\tau_i} + (\tau_E\,\underline{G} - \underline{C})e^{-t/\tau_E}\right]\right\}\underline{I}$$

Writing the matrices in detail and simplifying gives

$$\xrightarrow[22,23,24,34,36]{40} (41) \qquad \begin{vmatrix} V_{Ii}(t) \\ V_{IE}(t) \end{vmatrix} = \frac{I_g}{G_i G_E}\left\{\begin{vmatrix} G_l \\ G_i \end{vmatrix} + \frac{1}{\tau_i - \tau_E} \times \left[\left(-\tau_i \begin{vmatrix} G_l \\ G_i \end{vmatrix} + \begin{vmatrix} C_l \\ C_i \end{vmatrix}\right)e^{-t/\tau_i} + \left(\tau_E \begin{vmatrix} G_l \\ G_i \end{vmatrix} - \begin{vmatrix} C_l \\ C_i \end{vmatrix}\right)e^{-t/\tau_E}\right]\right\}$$

IV. CHARACTERISTICS OF THE SOLUTION

Prior to breakdown, the voltage across the external node pair is

$$\xrightarrow[36]{41} (42) \qquad V_{IE}(t) = \frac{I_g}{G_E}\left(1 - e^{-t/\tau_E}\right)$$

and the voltage across the internal node pair is

$$\xrightarrow{41} (43) \quad V_{Ii}(t) = \frac{G_l I_g}{G_i G_E}\left[1 + \frac{\tau_l - \tau_i}{\tau_i - \tau_E} e^{-t/\tau_i} - \frac{\tau_l - \tau_E}{\tau_i - \tau_E} e^{-t/\tau_E}\right]$$

where

$$\xrightarrow{\text{sym def}} (44) \qquad \tau_l = C_l/G_l$$

If breakdown does not occur, the asymptotic voltages approached are

$$\xrightarrow[t \to \infty]{42} (45) \qquad V_{IE\infty} = \frac{I_g}{G_E}$$

and

$$\xrightarrow[t \to \infty]{43} (46) \qquad V_{Ii\infty} = \frac{G_l}{G_i} V_{IE\infty}$$

as can be obtained directly from Fig. D1 by disregarding the capacitances.

Because of the large number of parameters involved, it is convenient to normalize all time quantities with respect to a particular time constant. Since τ_i is the easiest one to determine, it is used for the normalized unit of time. Thus,

$$\xrightarrow{\text{sym def}} (47) \qquad \begin{bmatrix} T \\ T_E \\ T_l \end{bmatrix} = \frac{1}{\tau_i} \begin{bmatrix} t \\ \tau_E \\ \tau_l \end{bmatrix}$$

In terms of normalized time,

$$\xrightarrow[47]{43} (48) \quad V_{Ii}(T) = \frac{G_l I_g}{G_i G_E}\left[1 + \frac{T_l - 1}{1 - T_E} e^{-T} - \frac{T_l - T_E}{1 - T_E} e^{-T/T_E}\right]$$

Of particular interest is the maximum value of the input voltage V_{Ii}, and the time it takes to occur $t_\wedge$. The voltage V_E is also of interest because its behavior determines when breakdown occurs, initiating a discharge phase of the cycle.

$$\xrightarrow{48} (49) \quad \frac{dV_{Ii}}{dT} = \frac{G_l}{G_i G_E} \frac{I_g}{1 - T_E}\left[(1 - T_l) e^{-T} + \left(\frac{T_l}{T_E} - 1\right) e^{-T/T_E}\right]$$

At

$$\xrightarrow{\text{sym def}} (50) \qquad T = T_\wedge = \text{the normalized time at which the maximum occurs}$$

the time derivative of the voltage is zero, and hence,

$$\xrightarrow{49} (51) \quad (1 - T_l) e^{-T_\wedge} = \left(1 - \frac{T_l}{T_E}\right) e^{-T_\wedge/T_E}$$

Hence,

$$\xrightarrow{51} (52) \qquad e^{T_\wedge (T_E^{-1} - 1)} = \frac{T_l T_E^{-1} - 1}{T_l - 1}$$

and thus,

$$\xrightarrow{52} (53) \qquad T_\wedge = \frac{1}{T_E^{-1} - 1} \ln \frac{T_l T_E^{-1} - 1}{T_l - 1}$$

The maximum voltage is

$$\xrightarrow[53]{48} (54) \quad \hat{V}_{Ii} = \frac{G_l I_g}{G_i G_E}\left[1 + \frac{T_l - 1}{1 - T_E}\left(\frac{T_l T_E^{-1} - 1}{T_l - 1}\right)^{1/(1 - T_E^{-1})} - \frac{T_l - T_E}{1 - T_E}\left(\frac{T_l T_E^{-1} - 1}{T_l - 1}\right)^{1/(T_E - 1)}\right]$$

Normalizing with respect to the asymptotic voltage,

$$\xrightarrow[45]{46} (55) \qquad \hat{V}_{Ii\infty} = \frac{G_l I_g}{G_i G_E}$$

and simplifying gives

$$\xrightarrow[55]{54} (56) \frac{\hat{V}_{Ii}}{V_{Ii\infty}} = 1 + \frac{1}{1 - T_E} \frac{(T_l T_E^{-1} - 1)^{T_E/(T_E - 1)}}{(T_l - 1)^{1/(T_E - 1)}} - \frac{T_E}{1 - T_E} \frac{(T_l T_E^{-1} - 1)^{T_E/(T_E - 1)}}{(T_l - 1)^{1/(T_E - 1)}}$$

Hence,

$$\xrightarrow{56} (57) \qquad \frac{\hat{V}_{Ii}}{V_{Ii\infty}} = 1 + \frac{(T_l T_E^{-1} - 1)^{T_E/(T_E - 1)}}{(T_l - 1)^{1/(T_E - 1)}}$$

It should be noted that $V_{Ii\infty}$ is also a function of quantities which enter the time constant; hence, this ratio can be somewhat misleading in certain circumstances. The asymptotic input voltage is plotted in Fig. D2 against the asymptotic external voltage, with R_i/R_l as the parameter identifying each curve. The graph can also be interpreted with R_iI_g as the abscissa (the asymptotic voltage developed across the input terminals of the electronic device if all of the generator current passed into the electronic circuit), with R_E/R_l as the parameter identifying each curve.

The time at which the maximum occurs (normalized with respect to the electronic circuit input-impedance time constant) is plotted against the external environment charging time constant (also normalized with respect to τ_i) for various leakage time constants (also normalized with respect to τ_i) in Fig. D3. The time to voltage peak becomes relatively large as the external time constant approaches the leakage time constant. The ratio of the peak input voltage to the asymptotic voltage is shown as a function of the time constants in Fig. D4. Very large ratios occur for large values of the leakage time constant. These curves must be used in conjunction with Fig. D2 for meaningful interpretation, especially for large values to T_l which may have accompanying small values of asymptotic voltage. For these cases, it would be more appropriate to normalize the peak voltage with respect to R_iI_g or R_EI_g rather than to the asymptotic voltage.

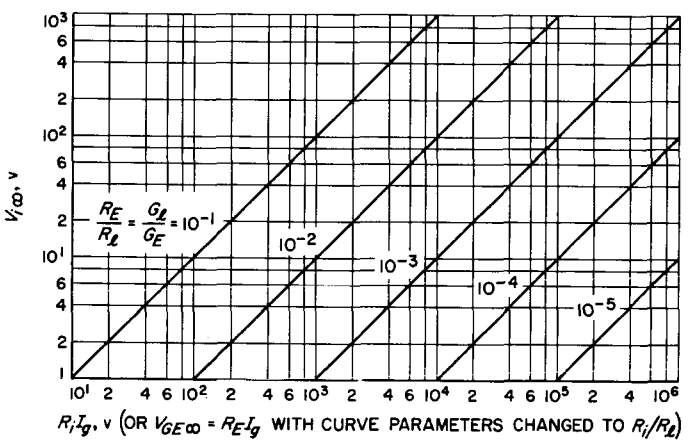

Fig. D2. Asymptotic voltage produced across input impedance by electrostatic charging, if breakdown does not occur

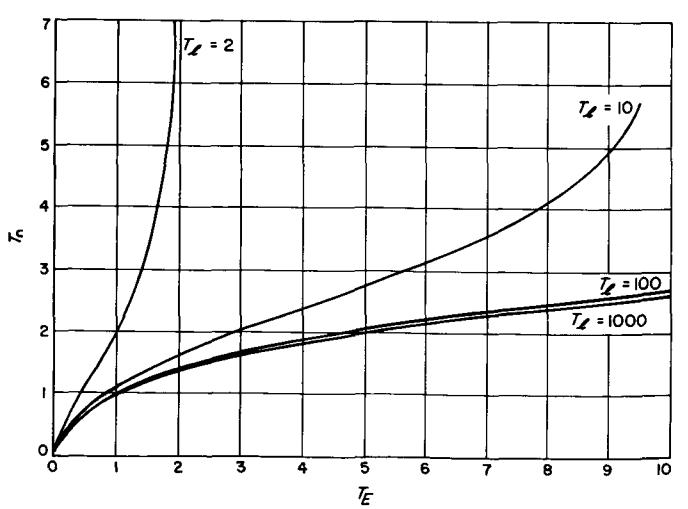

Fig. D3. Normalized time-to-peak vs normalized external time constant

$$\xrightarrow{57} \quad (58)\ \widehat{V}_{Ii} - V_{Ii\infty} = V_{Ii\infty}\,\frac{(T_lT_E^{-1} - 1)^{T_E/(T_E-1)}}{(T_l - 1)^{1/(T_E-1)}}$$

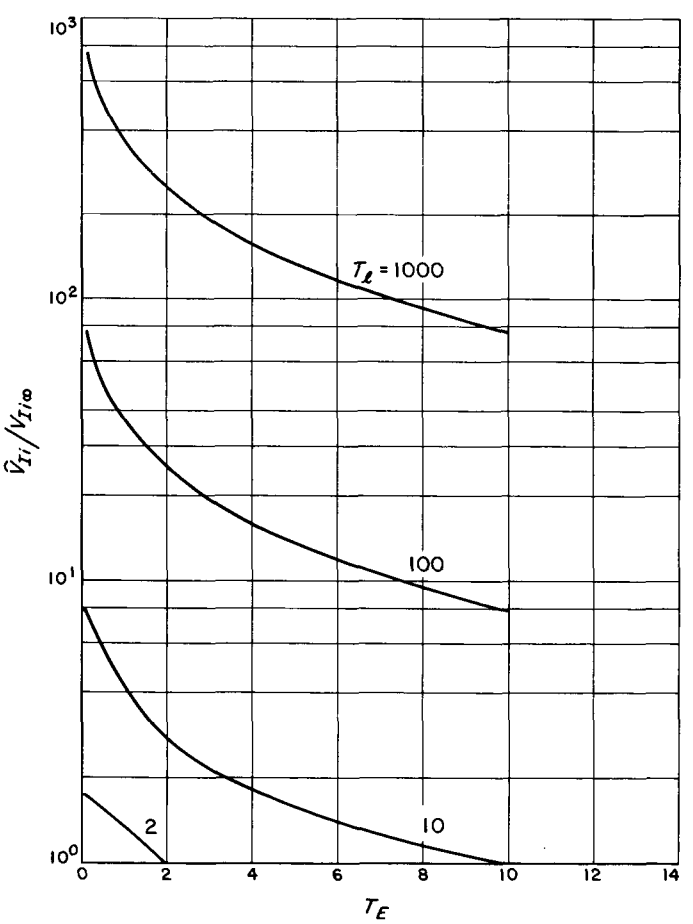

Fig. D4. Normalized peak voltage vs normalized external time constant

Of particular interest is the case for which the leakage conductance is sufficiently small to be completely neglected. For this case, $V_{Ii\infty}$ becomes zero and the right-hand side of (58) becomes indeterminant; hence, an alternate form is more appropriate. Since T_l becomes infinite as G_l becomes zero, a more appropriate form is

$$\xrightarrow[55]{58} (59) \qquad \hat{V}_{Ii} - V_{Ii\infty} = \frac{G_l I_g}{G_i G_E} \frac{T_l}{T_E^{T_E/(T_E-1)}} \frac{(1 - T_E T_l^{-1})^{T_E/(T_E-1)}}{(1 - T_l^{-1})^{1/(T_E-1)}}$$

Eliminating the cancelling G_l's gives

$$\xrightarrow[47,\,44,\,24]{59} (60) \qquad \hat{V}_{Ii} - V_{Ii\infty} = \frac{C_l I_g}{C_i G_E} T_E^{-T_E/(T_E-1)} \frac{(1 - T_E T_E^{-1})^{T_E/(T_E-1)}}{(1 - T_l^{-1})^{1/(T_E-1)}}$$

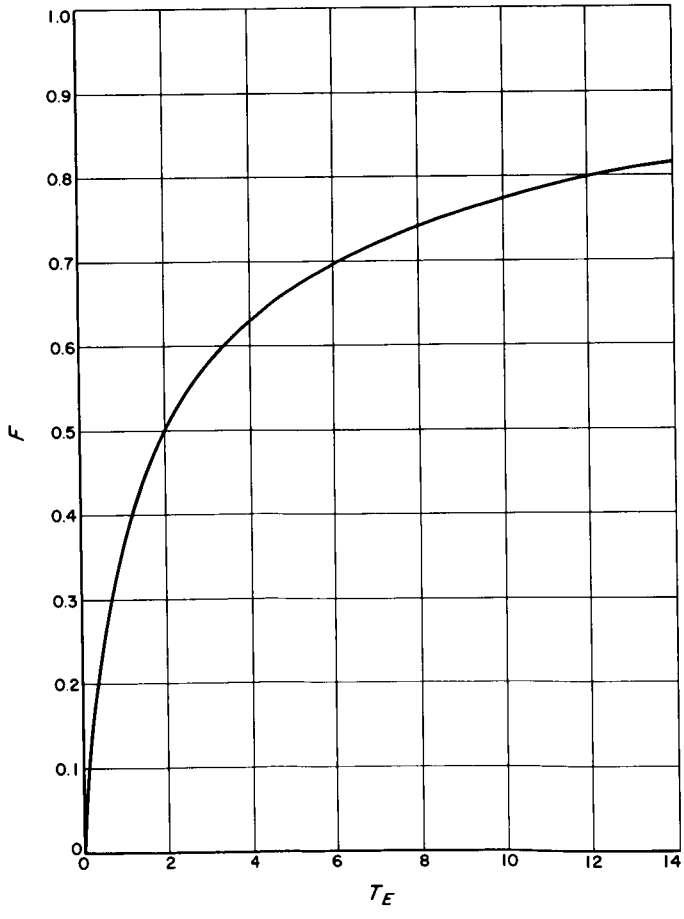

Fig. D5. Parameter F vs T_E

Using

$$\xrightarrow{\text{sym def}} (61) \qquad \hat{V}_{Ii}^* = \lim_{G_l \to 0} \hat{V}_{Ii}$$

gives

$$\xrightarrow{60} (62) \qquad \hat{V}_{Ii}^* = \frac{C_l}{C_i} \frac{I_g}{G_E} T_E^{-T_E/(T_E-1)}$$

An alternate form, which is more useful for graphical presentation, is

$$\xrightarrow[44,\,24]{62} (63) \qquad \hat{V}_{Ii}^* = \frac{C_l}{C_i} \frac{I_g}{G_i} T_E^{(T_E-1)^{-1}}$$

Since G_i is a better known quantity than G_E, this form is more advantageous because of the relatively slow variation for the factor

$$\xrightarrow{\text{sym def}} (64) \qquad F(T_E) = T_E^{(T_E-1)^{-1}}$$

This factor is plotted in Fig. D5. It should be noted that

$$\xrightarrow{\text{L'Hospital}} (65) \quad \lim_{T_E \to 0} F(T_E) = \exp \lim_{T_E \to \infty} \frac{\ln T_E}{1 - T_E} = \exp \lim_{T_E \to \infty} \frac{-1}{T_E} = 1$$

The peak voltage for the $G_l = 0$ case is plotted in Fig. D6 against $R_i I_g$ for various values of $(C_l/C_E)\,F$.

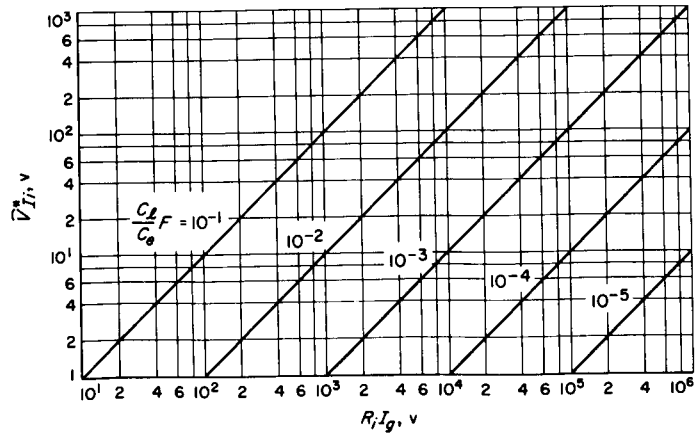

Fig. D6. Peak voltage vs input resistance times generator current for various parameter combinations (for $G_l = 0$)

It is convenient to compare the case without leakage to the case with leakage. Normalizing with respect to $\hat{V}_{Ii}^*$ gives

$$\xrightarrow{60 \div 62} (66) \quad \frac{\hat{V}_{Ii} - V_{Ii\infty}}{\hat{V}_{Ii}^*} = \frac{(1 - T_E T_l^{-1})^{T_E/(T_E-1)}}{(1 - T_l^{-1})^{1/(T_E-1)}}$$

Three particular points which facilitate sketching this function are

$$\xrightarrow{66} (67) \quad \lim_{T_E \to 0} \frac{\hat{V}_{Ii} - V_{Ii\infty}}{\hat{V}_{Ii}^*} = 1 - T_l^{-1}$$

$$\xrightarrow{66} (68) \quad \lim_{T_E \to 1} \frac{\hat{V}_{Ii} - V_{Ii\infty}}{\hat{V}_{Ii}^*} = (1 - T_l^{-1})\, e^{(1-T_l)^{-1}}$$

and

$$\xrightarrow{66} (69) \quad \lim_{T_E \to T_l} \frac{\hat{V}_{Ii} - V_{Ii\infty}}{\hat{V}_{Ii}^*} = 0$$

For very large values of T_l, the expression reduces to

$$\xrightarrow[T_l >> 1]{66} (70) \quad \frac{\hat{V}_{Ii} - V_{Ii\infty}}{\hat{V}_{Ii}^*} = \left(1 - \frac{T_E}{T_E - 1}\frac{T_E}{T_l} - \ldots\right)\left(1 + \frac{1}{T_E - 1}\frac{1}{T_l} + \ldots\right)$$

and hence, to

$$\xrightarrow{70} (71) \quad \frac{\hat{V}_{Ii} - V_{Ii\infty}}{\hat{V}_{Ii}^*} = 1 - \frac{T_E + 1}{T_l}$$

The difference between the peak and asymptotic voltage normalized with respect to the peak voltage for the case of no leakage conductance is shown in Fig. D6.

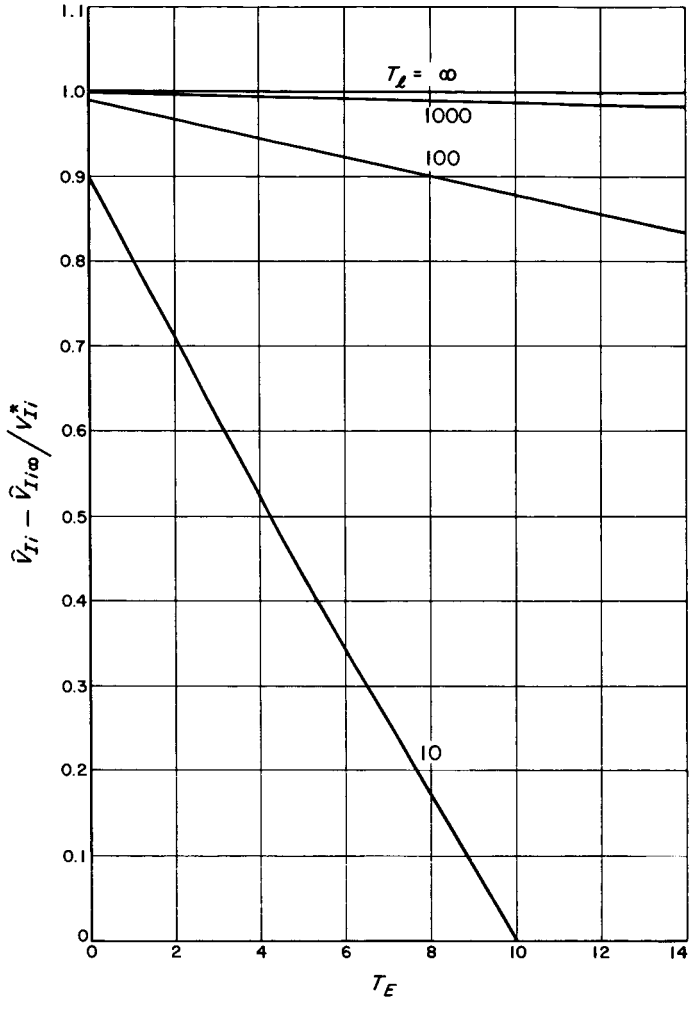

Fig. D7. Peak voltage less asymptotic voltage (normalized with respect to peak voltage) vs normalized external time constant (for $G_l = 0$)

APPENDIX E

Analysis of Equivalent Discharging Circuit

During a flashover discharge, the external portion of the equivalent circuit is essentially short-circuited. Thus, the equivalent circuit for the discharge mode reduces to that depicted in Fig. E1. The voltage across the input can be obtained from the node equation

$$\xrightarrow{\text{Fig E1}} \quad (1) \qquad (G_l + G_i)\,V_i + (C_l + C_i)\,\dot{V}_i = 0$$

Taking the Laplace transform gives

$$\xrightarrow{\text{1, Tab D1}} \quad (2) \qquad [(G_l + G_i) + (C_l + C_i)s]\,\bar{V}_i = (C_l + C_i)\,V_i(0)$$

Solving for the voltage transform gives

$$\xrightarrow{2} \quad (3) \qquad \bar{V}_i = \frac{V_i(0)}{s + \dfrac{1}{\tau_d}}$$

where

$$\xrightarrow{\text{sym def}} \quad (4) \qquad \tau_d = \frac{C_i + C_l}{G_i + G_l}$$

is the discharge time constant. Under the normally prevailing conditions, the leakage current parameters are small compared to the input circuit parameter. Consequently,

$$\xrightarrow[\text{D-32, D-33}]{4} \quad (5) \qquad \tau_d = \tau_i$$

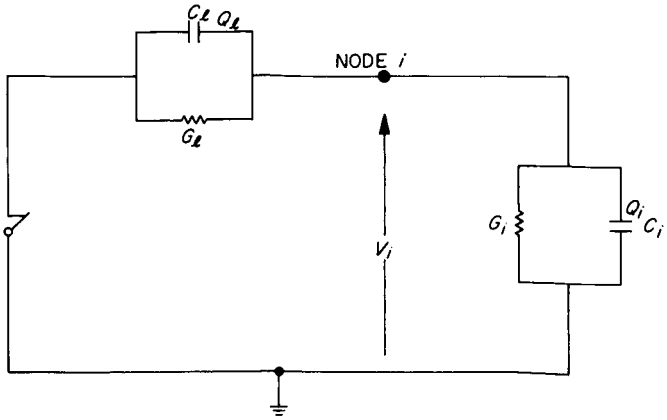

Fig. E1. Reduced equivalent circuit for discharge mode

Taking the inverse transform gives

$$\xrightarrow[5]{\text{3, Tab D1}} \quad (6) \qquad V_i(t) = V_{io}\,e^{-t/\tau_i}$$

The initial voltage is given in terms of

$$\xrightarrow{\text{sym def}} \quad (7) \qquad Q_{io} = \text{the initial charge on } C_i$$

and

$$\xrightarrow{\text{sym def}} \quad (8) \qquad Q_{lo} = \text{the initial charge on } C_l$$

by

$$\xrightarrow{\text{Fig E1}} \quad (9) \qquad V_{io} = \frac{Q_{io} + Q_{lo}}{C_i + C_l}$$

The initial charge on the internal capacitance is

$$\xrightarrow{\text{Fig D1}} \quad (10) \qquad Q_{io} = C_i\,V_{iB}$$

where

$$\xrightarrow{\text{sym def}} \quad (11) \qquad V_{iB-} = \text{the input voltage just preceding breakdown}$$

The initial charge on the leakage capacitance is

$$\xrightarrow{\text{Fig D1}} \quad (12) \qquad Q_{lo} = C_l\,(V_{iB-} - V_{EB-})$$

where

$$\xrightarrow{\text{sym def}} \quad (13) \qquad V_{EB-} = \text{the external node voltage just preceding breakdown}$$

The initial input voltage for the discharge phase can thus be expressed by

$$\xrightarrow[10, 12]{9} \quad (14) \qquad V_{io} = V_{iB-} - \frac{C_l}{C_i + C_l}\,V_{EB-}$$

Since the leakage capacitance is small compared to the input capacitance,

$$\xrightarrow[\text{D-32}]{14} \quad (15) \qquad V_{io} = V_{iB-} - \frac{C_l}{C_i}\,V_{EB-}$$

If the leakage conductance is negligible, the largest initial voltage is obtained if breakdown occurs just prior to establishment of equilibrium in the charging mode. Thus,

$$\xrightarrow[V_{iB-}=0]{15} \quad (16) \qquad \hat{V}_{io} = -\frac{C_l}{C_i} V_{EB-}$$

This is shown graphically in Fig. E2.

The total charge which flows through the input resistance (if G_l is negligible) is the initial charge stored on C_l and C_i

$$\xrightarrow{\text{Fig E1}} \quad (17) \qquad Q_{R_i\infty} = Q_{io} + Q_{lo}$$

Hence,

$$\xrightarrow[10,\,12]{17} \quad (18) \qquad Q_{R_i\infty} = (C_i + C_l)\, V_{iB-} - C_l\, V_{EB-}$$

With the same approximations as employed before, the maximum charge which passes through R_i is

$$\xrightarrow{18} \quad (19) \qquad \hat{Q}_{R_i\infty} = -\, C_l\, V_{EB-}$$

This is shown graphically in Fig. E3.

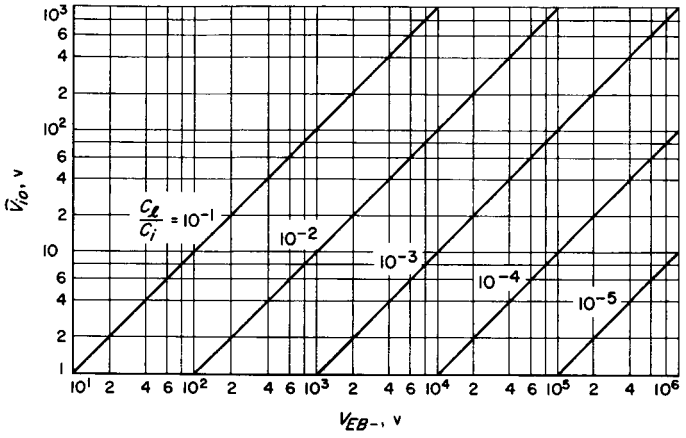

Fig. E2. Maximum input voltage vs breakdown voltage

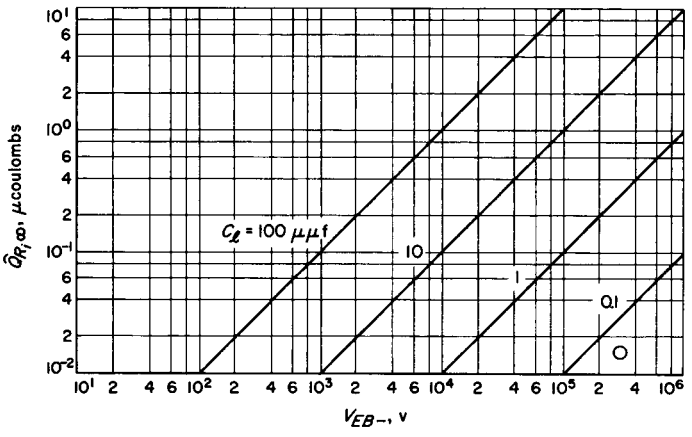

Fig. E3. Maximum input charge vs breakdown voltage

REFERENCES

1. *American Institute of Physics Handbook*, 2nd edition, New York: McGraw-Hill Book Co., Inc., 1963.
2. Smyth, W. R., *Static and Dynamic Electricity*, 2nd edition, New York: McGraw-Hill Book Co., Inc., 1950.
3. Delcroix, J. L., "Introduction to the Theory of Ionized Gases," *Interscience Tracts on Physics and Astronomy*, No. 8, 1960.